Published in final edited form as:
*Meteorit Planet Sci*. 2019 November 1; 54(11): 2666–2685. doi:10.1111/maps.13379.

# Oxygen isotope systematics of chondrule olivine, pyroxene, and plagioclase in one of the most pristine $CV3_{Red}$ chondrites (Northwest Africa 8613)

**Andreas T. Hertwig**[1,3,*], **Makoto Kimura**[2], **Céline Defouilloy**[1], **Noriko T. Kita**[1]

[1]WiscSIMS, Department of Geoscience, University of Wisconsin-Madison, Madison, WI 53706, USA

[2]National Institute of Polar Research, Meteorite Research Center, Midoricho 10-3, Tachikawa, Tokyo 190-8518, Japan

[3]Present address: Department of Earth, Planetary, and Space Sciences, University of California-Los Angeles, Los Angeles, CA 90095, USA

## Abstract

We performed in situ oxygen three-isotope measurements of chondrule olivine, pyroxenes, and plagioclase from the newly described $CV_{Red}$ chondrite NWA 8613. Additionally, oxygen isotope ratios of plagioclase in chondrules from the Kaba $CV3_{OxB}$ chondrite were determined to enable comparisons of isotope ratios and degree of alteration of chondrules in both CV lithologies.

NWA 8613 was affected by only mild thermal metamorphism. The majority of oxygen isotope ratios of olivine and pyroxenes plot along a slope-1 line in the oxygen three-isotope diagram, except for a type II and a remolten barred olivine chondrule. When isotopic relict olivine is excluded, olivine, low- and high-Ca pyroxenes are indistinguishable regarding $\Delta^{17}O$ values. Conversely, plagioclase in chondrules from NWA 8613 and Kaba plot along mass-dependent fractionation lines. Oxygen isotopic disequilibrium between phenocrysts and plagioclase was caused probably by exchange of plagioclase with $^{16}O$-poor fluids on the CV parent body.

Based on an existing oxygen isotope mass balance model, possible dust enrichment and ice enhancement factors were estimated. Type I chondrules from NWA 8613 possibly formed at moderately high dust enrichment factors (50× to 150× CI dust relative to Solar abundances); estimates for water ice in the chondrule precursors range from 0.2 to 0.6× the nominal amount of ice in dust of CI composition. Findings agree with results from an earlier study on oxygen isotopes in chondrules of the Kaba CV chondrite, providing further evidence for a relatively dry and only moderately high dust-enriched disk in the CV chondrule-forming region.

## 1. Introduction

Most chondritic meteorites contain chondrules - globular, once-molten objects often comprising olivine and low-Ca pyroxene phenocrysts in addition to glassy or crystalline

*corresponding author: hertwig@ucla.edu.

mesostasis (Hewins 1996; Brearley and Jones 1998; Scott and Krot 2007). Chondrules formed through ephemeral high-temperature events in the protoplanetary disk (Grossman 1988; Rubin 2000; Connolly, Jr. and Desch 2004) some 1-4 m.y. after CAI formation (Kita et al. 2005; Krot et al. 2009; Villeneuve et al. 2009; Kleine and Rudge 2011; Kita and Ushikubo 2012). Recent in-situ SIMS analyses of chondrules from various groups of carbonaceous chondrites demonstrated that mean chondrule $\Delta^{17}O$ values ($=\delta^{17}O - 0.52\times\delta^{18}O$) typically fall in the range between −10‰ and 0‰ (e.g., Jones et al. 2004; Chaussidon et al. 2008; Connolly and Huss 2010; Libourel and Chaussidon 2011; Rudraswami et al. 2011; Ushikubo et al. 2012; Schrader et al. 2013, 2014; Tenner et al. 2013, 2015, 2017; Hertwig et al. 2018). On the familiar oxygen three-isotope diagram, many chondrule phenocrysts plot along a slope-1 line (e.g., Jones et al. 2004; Rudraswami et al. 2011; Ushikubo et al. 2012; Schrader et al. 2013; Tenner et al. 2017) such as the PCM (primitive chondrule minerals, Ushikubo et al. 2012) or CCAM (Clayton et al. 1977; Clayton 1993, 2008) lines. On the other hand, minerals in chondrules from ordinary chondrites usually plot along a mass-dependent trend parallel to - and slightly above - the terrestrial fractionation (TF) line (e.g., Kita et al. 2010).

Most chondrules are internally homogeneous, i.e., olivine and pyroxenes are indistinguishable in terms of $\Delta^{17}O$ values given the relevant analytical uncertainty limits (e.g., Rudraswami et al. 2011; Ushikubo et al. 2012; Tenner et al. 2013, 2015, 2017; Hertwig et al. 2018). Internal homogeneity of chondrules indicates that minerals probably formed from a homogenized final chondrule-forming melt and, therefore, that the corresponding mean oxygen isotope ratios of chondrules reflect those of the final melt (e.g., Ushikubo et al. 2012; Tenner et al. 2013, 2015). Although the majority of chondrules comprise isotopically indistinguishable phenocrysts, some contain relicts of olivine grains that resisted complete melting. Relict olivine can be apparent within chondrules, e.g., in the form of dusty olivine grains or forsteritic olivine cores in FeO-rich chondrules (e.g., Nagahara 1983; Jones 1996; Wasson and Rubin 2003); they have also been identified by SIMS oxygen isotope analysis because of distinctly different oxygen isotope ratios in comparison with other grains within the same chondrules (Kunihiro et al. 2004, 2005; Krot et al. 2006; Ruzicka et al. 2007; Rudraswami et al. 2011; Ushikubo et al. 2012; Tenner et al. 2013). Prior studies on chondrules in pristine chondrites with minimal aqueous alteration have shown the oxygen isotope ratios of glass and/or plagioclase to be indistinguishable from those of chondrule phenocrysts (Ushikubo et al. 2012; Tenner et al. 2015, 2017). This is not the case, however, in chondrites that show evidence of aqueous alteration (Semarkona, Kita et al. 2010; Allende, Rudraswami et al. 2011; Kaba, Krot and Nagashima 2016).

While mean oxygen isotope ratios of chondrules provide constraints on the effective isotopic composition of the chondrule-forming melt (e.g., Ushikubo et al. 2012; Tenner et al. 2015), mean Mg#'s of chondrule phenocrysts allow for estimating redox conditions (e.g., Ebel and Grossman 2000; Krot et al. 2000; Tenner et al. 2015). The mean Mg# of a chondrule (MgO/[MgO+FeO], mol.%) is calculated by averaging the Mg#'s of all ferromagnesian mineral phases and is, to a first approximation, a function of the oxygen fugacity $f_{O_2}$ of the melt (e.g., Tenner et al. 2015) given that Fe-availability does not become a limiting factor. The $f_{O_2}$-conditions that permit the formation of chondrules with Mg# ~98, such as those common in carbonaceous chondrites, are considerably higher (i.e., more oxidizing; $\log(f_{O_2})$: IW – 2)

than thought plausible in the canonical Solar nebula (e.g., $\log(f_{O2})$: ~ IW – 6 at 1600 K, Krot et al. 2000). As discussed comprehensively by Ebel and Grossman (2000), the local oxygen fugacity of the protoplanetary disk can be higher if the disk is enriched in dust of CI composition relative to Solar abundances. Furthermore, accumulation of $H_2O$ ice in the chondrule-forming region would significantly raise the oxygen fugacity (e.g., Connolly and Huss 2010; Schrader et al. 2013; Tenner et al. 2015).

Based on the calculations of Ebel and Grossman (2000), Tenner et al. (2015) developed a model that facilitates estimation of dust enrichment and ice enhancement factors (relative to Solar nebula compositions) via mean chondrule Mg#'s and $\Delta^{17}O$ values. Initially developed for CR chondrites, this model has been recently applied to chondrules of the Kaba CV chondrite, yielding moderately high dust enrichment factors (50×–100× CI dust) and a low water ice abundance in the precursor dust (0-0.6× of the nominal ice in dust of CI composition, Hertwig et al. 2018). Similar to CR chondrites, the $\Delta^{17}O$ values of chondrules from Kaba tend to increase with decreasing Mg#'s although the trend is less pronounced due to higher and less variable Mg#'s of Kaba's type I chondrules (Hertwig et al. 2018).

Vigarano-type carbonaceous chondrites (CV) are sub-divided into oxidized and reduced groups ($CV_{Ox}$ and $CV_{Red}$, respectively) (McSween 1977); oxidized CV chondrites comprise magnetite and Ni-rich sulfides as predominant opaque phases, while metal alloys and troilite are the primary opaque phases in reduced CV chondrites (e.g., McSween 1977; Krot et al. 1995). Further, oxidized CV chondrites are subdivided into the Bali-like ($CV_{OxB}$) and Allende-like ($CV_{OxA}$) subgroups (Weisberg et al. 1997). Phyllosilicates, likely the products of hydrous alteration on the CV parent body, are abundant in chondrules of oxidized Bali-like CVs but absent in reduced CV chondrites (Keller and Buseck 1990; Kimura and Ikeda 1998; Krot et al. 1998). Kaba is a member of the Bali-like oxidized subgroup of CV chondrites and $\Delta^{17}O$ values of Kaba chondrules are broadly consistent with those from Allende ($CV_{OxA}$) (Hertwig et al. 2018). Unlike Kaba (CV3.1, Grossman and Brearley 2005; Bonal et al. 2006), Allende experienced significant thermal metamorphism (e.g., Bonal et al. 2006) that caused secondary, diffusion-related FeO zonation in olivine and complicates comparison of chondrule Mg#'s between both chondrites. It is plausible that the primary, undisturbed $\Delta^{17}O$-Mg# systematics of CV chondrites is recorded in Kaba chondrules. General statements regarding the CV chondrule-forming environment are hindered, however, by a lack of systematic isotope studies of chondrules of the reduced CV chondrites.

To fill this gap, we performed SIMS oxygen three-isotope analyses of chondrules from the $CV_{Red}$ Northwest Africa (NWA) 8613. In terms of thermal metamorphism, chondrules of NWA 8613 were less affected than those of the $CV_{OxA}$ group and experienced less aqueous alteration compared to chondrules of the $CV_{OxB}$ group. NWA 8613 is a rare reduced CV with a low shock stage and a relatively low petrologic subtype (3.1-3.2), which makes this meteorite one of the most pristine CV chondrites described so far (Sato et al. 2016). We report detailed descriptions of chondrules in NWA 8613 and their oxygen isotope systematics, which are compared to those of the Kaba and Allende CV3 chondrites reported in previous studies (Hertwig et al. 2018; Rudraswami et al. 2011). Using these data, dust enrichment as well as ice enhancement factors of the CV chondrule-forming region are estimated. We further performed oxygen three-isotope analyses of plagioclase in chondrules

of NWA 8613, as the oxygen isotope ratios of plagioclase are particularly sensitive to parent body processes (Rudraswami et al. 2011; Krot and Nagashima 2016). We also analyzed plagioclase in selected chondrules of Kaba to evaluate how oxygen isotopes in plagioclase behave at different degrees of parent body alteration.

## 2. Analytical techniques

### 2.1. Sample description

General petrographic features of NWA 8613 have been previously described in a conference abstract by Sato et al. (2016); a summary of their work is provided here. NWA 8613 was purchased in 2013 and classified as reduced CV chondrite (Meteoritical Bulletin No. 103; Ruzicka et al. 2017). A low petrologic subtype (3.1-3.2) was suggested based on mineral textures indicative of only minor alkali-calcium exchange in the mesostasis (nepheline lamellae), scarce secondary zoning in chondrule olivine, and no alteration of low-Ca pyroxene. The particular thin section analyzed in this study (NWA 8613-1, from the collection of the Ibaraki University, Japan) comprises ~41.2 vol.% chondrules (apparent average diameter : 0.84 mm), ~45 vol.% matrix, and 13.8 vol.% refractory inclusions with the latter being primarily type A CAIs and AOAs. NWA 8613 is unshocked (S1) as shown by aspect ratios of chondrules and only moderately weathered (W3).

### 2.2. Electron Microscopy

The NWA 8613-1 thin section and individual chondrules were examined by back-scattered electron (BSE) and secondary electron (SE) images using the Hitachi S-3400N SEM at the Department of Geoscience, UW-Madison. For a first assessment of the mineral chemistry of chondrule minerals including opaque phases, semi-quantitative energy dispersive X-ray spectrometer (EDS) analysis were carried out utilizing the NORAN System SIX analytical system and, after an upgrade of the Hitachi SEM, the AzTecEnergy X-ray analysis system (x-act detector). For the Kaba 1052-1 thin section, we fall back on BSE/SE imaging done earlier (see Appendix of Hertwig et al. 2018). Detailed BSE and SE images were used to select locations of SIMS analyses. After oxygen isotope analysis, the quality of each individual SIMS pit was evaluated by SEM imaging. This includes new SIMS pits in plagioclase of chondrules in the Kaba 1052-1 thin section.

Quantitative analyses of the chemical composition of olivine and pyroxenes (focused beam, 20 nA, 15keV), and plagioclase (5 μm, 10nA, 15keV) were performed using the Cameca SXFive FE electron microprobe hosted at the Department of Geoscience, UW-Madison. Concentrations of the following major and minor oxides were measured: $SiO_2$, $TiO_2$, $Al_2O_3$, $Cr_2O_3$, MgO, FeO, MnO, CaO, $K_2O$, and $Na_2O$. Counting times were 10s on the peak and 5s on the background. In the order listed above, analyte detection limits ($3\sigma$) in olivine and pyroxenes were not exceeding 0.03, 0.05, 0.03, 0.05, 0.01, 0.05, 0.06, 0.01, 0.02, and 0.02 wt.%. The following minerals from the reference collection were used to calibrate the x-ray response of each analyzed element: $Fo_{90}$ or synthetic enstatite (Si); rutile (Ti); jadeite (Al); $Cr_2O_3$ (Cr); synthetic forsterite or enstatite (Mg); hematite (Fe); manganese olivine (Mn); wollastonite (Ca); microcline (K); jadeite (Na). Plagioclase analyses were performed using a defocused beam and the following minerals to calibrate the x-ray response: Andesine (Na,

Ca, Al, Si); synthetic forsterite (Mg); microcline (K); rutile (Ti); $Cr_2O_3$ (Cr); manganese olivine (Mn); fayalite (Fe). ZAF correction and data reduction were done with the "Probe for EPMA" software (Donovan 2015).

To evaluate the alteration state of the mesostasis, average compositions of chondrule mesostasis were determined by EPMA with a highly defocused beam (10 μm diameter, performed at NIPR, Japan) to analyze plagioclase together with nepheline lamellae and diopside (see Data S1 in supporting information).

### 2.3. SIMS oxygen isotope analysis

Oxygen isotope ratios of olivine and pyroxene were determined by in-situ SIMS oxygen three-isotope analysis utilizing the Cameca IMS 1280 SIMS at the UW-Madison and using multi-collector Faraday cups (FCs). Analytical routines were similar to those described in Kita et al. (2010) and Tenner et al. (2013). Further, precision of $\delta^{17}O$ analyses was improved by replacing the original FC amplifier board with a board originally designed for the IMS 1280-HR. The newer board is characterized by a low thermal noise which is close to the theoretical limit (Johnson-Nyquist noise). A primary $Cs^+$ beam of 3.0-3.5 nA was tuned to generate a ~12 μm diameter spot on the sample surface. Secondary $^{16}O^-$ ion intensities were ~$4\times10^9$ cps (counts per second). A single spot analysis took 4 minutes including 60 s baseline measurement, ~ 1 minutes of DTFA scan, and 100 s signal acquisition, which is about a half of previous studies (e.g. Kita et al. 2010). At the end of each analyses, the intensity of $^{16}O^1H^-$ was determined automatically to calculate the contribution of the tailing of the $^{16}O^1H^-$ to the $^{17}O^-$ peak. The resulting correction was always insignificant (< 0.1 ‰).

Oxygen isotope ratios of plagioclase in chondrules of NWA 8613 and Kaba were determined during a separate analytical session using the same analytical parameters cited above, except for a lower primary beam current (1.8-2.0 nA) which results in lower secondary intensity ($^{16}O^-$, ~ $2.5\times10^9$ cps) and slightly larger analytical uncertainties compared to olivine and pyroxene analyses.

In both sessions, analysis was performed in such a way that 8-18 analyses of unknowns were enclosed in one bracket of the San Carlos olivine standard (4 before, 4 standard analyses after the unknowns). Analytical uncertainties were determined by repeated analyses of the San Carlos olivine standard. For the first session (olivine and pyroxene), uncertainties for $\delta^{17}O$, $\delta^{18}O$, and $\Delta^{17}O$ were on the average ~0.3, ~0.2, and ~0.3‰ (2SD); for the second session (plagioclase in NWA 8613, Kaba), ~0.5, ~0.3, and ~0.6‰ (2SD). Instrumental biases in $\delta^{18}O$ for olivine and pyroxene analyses were calibrated using 3 olivine ($Fo_{100}$, $Fo_{89}$, $Fo_{60}$) and 4 pyroxene ($En_{97}$, $En_{89}$, $En_{85}$; $En_{50}Wo_{50}$) standards (Kita et al. 2010) with chemical compositions similar to those determined for the chondrule minerals of this study. For the second session, instrumental mass bias was calibrated using two plagioclase standards ($An_{90}$, $An_{60}$) (Valley and Kita 2009) that bracket the chemical composition of unknowns. Oxygen isotope ratios are reported relative to VSMOW (Baertschi 1976). Throughout this paper, analyses are identified by chondrule number followed by SIMS analysis number and mineral name.

### 2.4. Position of SIMS analyses

In NWA 8613, all chondrules with a clearly defined outline and diameters > ~1 mm were considered for SIMS analyses. Because of geometry constraints placed by the SIMS sample holder, some chondrules on the edge of the thin section were not available for SIMS measurements. In addition to chondrules > ~1 mm across, the only FeO-rich chondrule and two other chondrules with diameters < 1 mm were selected for SIMS analyses. All selected chondrules, labeled from N1 to N31, are shown in the BSE mosaic of the NWA 8613 thin section in Data S2. In each of these chondrules, at least 8 locations (preferably 4 olivine and 4 pyroxene) were chosen for SIMS measurements based on a thorough evaluation of high-resolution BSE and SE images. Locations free of cracks and inclusions were analyzed by EPMA to determine the mineral composition (see Data S3 for EPMA analyses) which is required to be known for instrumental bias correction of SIMS analysis. Subsequently, olivine and pyroxene were analyzed by SIMS for oxygen three-isotopes (complete SIMS data set in Data S5) followed by SEM imaging of individual SIMS pits in order to check whether pits are free of cracks or inclusions (see Data S6 for pit images). Based on this assessment, individual SIMS analyses were rejected from discussion (e.g., if pits hosting a significant number of cracks or inclusions were hit).

For oxygen isotope analysis of plagioclase, chondrules in NWA 8613 and Kaba were screened for plagioclase grains that can accommodate SIMS spots of ~10 μm (1-4 per chondrule). Further, plagioclase grains must be free of phyllosilicates and nepheline lamellae visible at ~1k magnification (NWA 8613). Crystallinity was confirmed by optical microscopy for some of the prospective SIMS locations. After SIMS analysis (see Data S2 for location of measurements), pits were evaluated by SEM imaging (see Data S7 for pit images).

### 2.5. Assessment of mean oxygen isotope ratios: data reduction scheme and corresponding analytical uncertainties

Mean chondrule isotope ratios were calculated using only olivine and pyroxene analyses. We closely follow the data reduction scheme previously described in detail by Hertwig et al. (2018). This iterative reduction theme draws upon previous work (Ushikubo et al. 2012; Tenner et al. 2013); a synopsis is provided here. Critical for the determination of the mean $\Delta^{17}O$ value is a criterion that allows for differentiating isotopically distinguishable analyses from a cluster of homogeneous analyses (with respect to $\Delta^{17}O$ values); the mean 3SD of San Carlos olivine analyses during the whole analytical session (±0.45 ‰) provides such a criterion. The mean chondrule $\Delta^{17}O$ value is defined as the mean of all individual analyses, if $\Delta^{17}O$ values are within the threshold of ±0.45 ‰ from the chondrule mean. If analyses of isotopic relict grains are present, a subset of analyses is selected that excludes these potential isotopic relicts but preferentially includes pyroxene analyses; thereof a new mean is calculated and tested for homogeneity with respect to the ±0.45 ‰ criterion. The last step is repeated until a subset of internally homogeneous analyses is found. The mean $\Delta^{17}O$ value should include at least 2 individual analyses per chondrule or the chondrule is called isotopically heterogeneous. The same analyses that are selected for calculating the mean $\Delta^{17}O$ values are also used for calculating the mean chondrule $\delta^{17}O$ and $\delta^{18}O$ values.

Uncertainties (unc.) for mean chondrule $\delta^{17}O$ and $\delta^{18}O$ values are propagated using the square root of the quadratic sum of (i) twice the standard error (2 SD/$\sqrt{n}$) considering those analyses that are included in the mean (SD: standard deviation of the unknowns or, when larger, the SD of the standard bracket), (ii) twice the standard error of those San Carlos olivine analyses that bracket the unknowns, and (iii) a constant value that takes into account the impact of the sample geometry and topography as well as the reproducibility of calibration standards on mean oxygen isotope ratios due to mass-dependent fractionation processes (±0.3‰ for $\delta^{18}O$, ±0.15‰ for $\delta^{17}O$, Kita et al. 2009). Uncertainties related to mean $\Delta^{17}O$ values are the sum of components (i) and (ii).

The 2SD of mean chondrule $\Delta^{17}O$ values of plagioclase describe the variation of analyses within individual chondrules. Mean $\delta^{17}O$ or $\delta^{18}O$ values have not been calculated.

## 3. Results

### 3.1. Petrography of chondrules in NWA 8613

Olivine and pyroxene from 31 chondrules were analyzed for oxygen three isotopes. Chondrules are FeO-poor (type I) except for one small fragmented FeO-rich chondrule (N16). The apparent diameter of analyzed chondrules ranges from 0.5 - 2.5 mm (longest dimension). Most of the chondrules (21 of 31, Fig. 1a-e,) are clearly defined, spherical masses, although some possess strongly frayed or otherwise irregular margins (10 of 31, Fig. 1f). In general, porphyritic textures (28 of 31) are predominant in relation to barred (2 of 31); Most chondrules are porphyritic olivine-pyroxene (POP) chondrules. One porphyritic olivine (PO) chondrule consists primarily of a single FeO-poor olivine fragment.

A closer look at porphyritic chondrules reveals a variety of textural features. For example, poikilitic low-Ca pyroxene laths form either complete (N1, N14; Fig. 1a,c; N7) or only partially enclosing shells (N2, Fig. 1b; N12) around chondrule interiors. These shells contain variable amounts of olivine and opaque phases; the latter are often concentrated near the interface with the chondrule interior, but can also be found dispersed within low-Ca pyroxene crystals (N14, N6; Fig. 1c,e). In the case of chondrules N13 and N20, low-Ca pyroxene in the shell is finer-grained and subordinate to olivine in abundance; these shells resemble igneous rims (e.g., Rubin 2000). In general, chondrule interiors surrounded by pyroxene shells are similar to granular (N12, Fig. 1h) or porphyritic olivine (N1, Fig 1a) and rarely comprise opaque phases (N14, Fig. 1c). Irregularly-shaped chondrules are opaque-phases-rich and can contain one or several clusters of PO material enclosed in low-Ca pyroxene (N17, N27, N29); one irregularly-shaped chondrule is composed entirely of poikilitic low-Ca pyroxene (N26), as is one roundish porphyritic pyroxene (PP) chondrule (N9). Some chondrules show adhesions of smaller chondrules (e.g., N12, Fig. 1h).

In terms of morphology, olivine in porphyritic chondrules occurs as anhedral to euhedral grains in mesostasis, irregularly-shaped grain aggregates, and as inclusions in low-Ca pyroxene. Although generally inclusions-free, olivine grains occasionally contain blobs of opaque phases. Olivine in the interior of chondrule N13 revealed trails of tiny metallic iron inclusions characteristic of “dusty” relict olivine. Cores of forsteritic relict olivine are

present in fayalitic olivine of the fragmented type II chondrule N16. In porphyritic chondrules, no replacement of pyroxene by ferroan olivine was observed.

Figure 2 illustrates the three most common types of mesostasis textures. In some chondrules, the mesostasis is devitrified and consists of high-Ca pyroxene (Hpx) dendrites embedded in plagioclase (Fig. 2a). As shown in Figure 2a and b, high-Ca pyroxene can occur as euhedral crystals in the mesostasis or form overgrowths on pyroxene of lower Ca content. Although the mesostasis in most chondrules is composed of anorthitic plagioclase and pyroxenes, 4 of the 31 chondrules (N14, N23, N27 N30) contain nepheline as an additional phase (Fig. 2c). Where present, nepheline forms thin (<1 μm) lamellae in anorthitic plagioclase and its abundance is low. No sodalite was observed in any of the chondrules.

Most commonly, the opaque mineral phases are dispersed within chondrules as either fine, roundish inclusions or as irregularly-shaped blobs. These phases were also observed concentrated at boundaries between textural zones or confined to the low-Ca pyroxene-rich shells. Noteworthy is a large aggregate sphere (0.8 mm in diameter) composed of various Fe-Ni-rich phases that is attached to chondrule N2 (Fig. 1b). This sphere is enveloped by the same incomplete pyroxene shell that rims the entire BO chondrule. Aggregates of opaque mineral phases also occur isolated in the chondrite matrix.

### 3.2. Chemical composition of chondrule minerals in NWA 8613 and plagioclase in Kaba

**Olivine—**Chemical analysis of olivine in type I chondrules yielded Mg#'s (or Fo content) in the range between 99.6 and 88.6 (96.3 ±4.9, 2SD, n=124). As can be seen in Figure 3, the Mg#'s can be variable within individual chondrules. On average, olivine with higher Mg#'s tends to have high CaO (Fig. 3a), $Al_2O_3$ (Fig. 3b), and $Cr_2O_3$ (Fig. 3c) contents while their MnO contents (Fig 3d) are close to or below the mean detection limit. Box charts of selected minor elements are presented in Data S8 in supporting information to illustrate the variation of those elements in different olivine grains of the same chondrule.

Olivine in the type II chondrule N16 yielded Mg#'s that range between 49.9 to 68.6, excluding forsteritic cores with Mg#'s of up to ~93. The $Cr_2O_3$ content was near detection limit (0.05 wt.%, 3SD), whereas MnO and CaO are present at average concentration of 0.3 wt.% and 0.2 wt.%, respectively (forsteritic cores included).

**Pyroxenes and plagioclase—**Alongside low-Ca pyroxene (defined as Wo < 3, where Wo = Ca/(Ca+Mg+Fe) × 100, mol.%), many chondrules contain intermediate (3 < Wo < 10) and/or high-Ca pyroxene (Wo > 10). For example, in chondrule N3, low-Ca pyroxenes (Wo ~ 1) are restricted to the opaque-phases-rich outer shell, while intermediate (Wo ~ 5) and high-Ca pyroxene are present in the mesostasis (Fig. 2b). Similarly, low-Ca pyroxene laths (Wo ~ 1) dominate the pyroxene shell of chondrule N1, whereas intermediate (Wo ~ 4 - 5) and high-Ca pyroxene (Wo ~ 39 - 44) occur in the chondrule interior (Fig. 1a). Pyroxenes are generally Fe-poor (Fs < 2, where Fs = Fe/(Fe+Mg+Ca) × 100, mol.%) with the exception of intermediate and high-Ca pyroxenes in the BO chondrule N15 (Fs ~ 7 - 9). Mean pyroxene Mg#'s from type I chondrules all exceed 98 (excluding chondrule N15) which contrasts with mostly lower mean olivine Mg#'s (Fig. 5). Ti and Al contents are lower in

low-Ca (Ti < 0.01, Al ~ 0.01 - 0.08, apfu, O = 6) and intermediate (Ti < 0.02, Al ~ 0.05 - 0.10) pyroxenes than in high-Ca pyroxenes (Ti ~ 0.2, Al ~ 0.1 - 0.4).

EPMA analyses (5 μm electron beam) of plagioclase in unaltered and nepheline-free chondrules of NWA 8613 yielded anorthite-rich compositions ($An_{78-85}$, An = Ca/(Ca+Na +K), mol.%). A separate set of EPMA measurements using a highly defocused beam (10 μm) confirmed small lamellae of nepheline in plagioclase of some of the chondrules in NWA 8613 (Fig. 4, see also Section 4.1.). Plagioclase in Kaba is nepheline-free but partly replaced by phyllosilicates in most chondrules (Hertwig et al. 2018); EPMA analyses of plagioclase in seven chondrules of Kaba show anorthite-rich compositions ($An_{83-95}$).

**Opaque phases—**In a subset of chondrules, the mineral chemistry of opaque phases was determined and all the evaluated chondrules contain either kamacite or taenite or both. In addition to alloys, chondrules contain troilite but pentlandite has been also described (Sato et al. 2016). Primary minerals are partly replaced by Fe,(Ni)-oxides and -oxyhydroxides, probably due to terrestrial weathering.

### 3.3. SIMS oxygen three-isotope analysis

**Oxygen three-isotope ratios of olivine and pyroxene in NWA 8613—**Excluding standard analyses, a total number of 262 SIMS oxygen three-isotope analyses were performed (olivine=137, pyroxene=125) of which 11 were rejected from discussion because of pit imperfections such as abundant cracks in the pit area. As shown in Figure 6, most olivine and pyroxene analyses plot on or slightly below the PCM line with $\delta^{17}O$ and $\delta^{18}O$ values ranging from −15‰ to −2‰ and −13‰ to −5‰ ($\Delta^{17}O$ ~ −9 - 0‰), respectively; one olivine is exceptionally $^{16}O$-rich (N17: 431.Ol; $\delta^{17}O$ ~ −32‰, $\delta^{18}O$ ~ −30‰; $\Delta^{17}O$ ~ −16‰). Contrary to oxygen isotope ratios of minerals in other chondrules, olivine and pyroxene in chondrule N13 yielded isotope ratios which consistently plot above the PCM line; analyses of the BO chondrule N15 also lie above the PCM but on the TF line. Some olivine grains in the type II chondrule N16 show fractionated oxygen isotope ratios with one analysis being located even below the CCAM line (Fig. 6).

**Oxygen three-isotope ratios of plagioclase in chondrules of NWA 8613 and Kaba—**Plagioclase in chondrules of both chondrites is clearly distinguishable from chondrule phenocrysts with respect to oxygen isotope ratios. Analyses plot below the TF line and isotope ratios vary between −1‰ and +7‰ for $\delta^{17}O$ and +5‰ and +15‰ for $\delta^{18}O$ (Fig. 7 and Tab. 1). Analyses in chondrules from Kaba closely follow a mass-dependent trend (sample mean: $\Delta^{17}O$ = −0.9 ±0.5‰, 2SD; see Fig. 7); plagioclase in NWA 8613 is more variable in ($\Delta^{17}O$ = −2.0 ±1.2‰, 2SD). The highest variability of chondrule plagioclase in terms of $\delta^{18}O$ values was observed in chondrules K1 of Kaba and N3 of NWA 8613 (analyses marked with an asterisk in Fig. 7).

**Distribution of $\Delta^{17}O$ values and relict olivine—**Figure 8 presents oxygen three-isotope diagrams illustrating the general isotopic characteristics of olivine, low-Ca, intermediate, and high-Ca pyroxene for selected chondrules of NWA 8613. Most chondrules (21 of 31, e.g., Fig. 8a-d) are isotopically homogeneous with respect to $\Delta^{17}O$ and the

homogeneity criterion of ±0.45‰ defined in Section 2.5, i.e., olivine and pyroxene in these chondrules are isotopically indistinguishable and isotopic relict grains were not observed. It can be seen in Figure 8e-h that intermediate and high-Ca pyroxene located mainly in the chondrule mesostasis possess $\Delta^{17}O$ values indistinguishable from olivine and low-Ca pyroxene phenocrysts in the respective chondrules.

Graphs in Figure 8h-l show isotope ratios of olivine and pyroxene for chondrules containing relict olivine (10 of 31 chondrules). In these chondrules, there exist at least 4 indistinguishable pyroxene and/or olivine analyses that define the respective mean chondrule $\Delta^{17}O$ values. Relict olivine is mostly $^{16}O$-rich (7 of 10 chondrules, e.g., Fig. 8h-j, l), spreads along the PCM line, and can occur in various textural positions. For example, some small olivine inclusions in low-Ca pyroxenes of chondrule N9 are $^{16}O$-rich with respect to their pyroxene hosts (Fig. 8j, 9a). Relict olivine also occurs as a massive grain aggregate that builds up most of the large (~ 2.5 mm diameter) chondrule N4 (see Data S2). This $^{16}O$-rich relict olivine is isotopically homogenous (Fig. 8i) and distinct from pyroxene and olivine in the chondrule rim. Texturally and isotopically remarkable dusty olivine is located in the interior of chondrule N13. Dusty olivine relicts are $^{16}O$-poor in comparison to minerals in the chondrule rim (Fig. 8h, 9b). Forsteritic olivine cores (Mg# ~90) in type II chondrule N16 are more $^{16}O$-rich than fayalitic olivine (Fig. 8l, 9c).

**Mean chondrule $\Delta^{17}O$ values of chondrules in NWA 8613—**Mean chondrule $\Delta^{17}O$ values were calculated using only olivine and pyroxene analyses and range from −6.7‰ to −0.1‰ (Fig. 10; Tab. 2; $\delta^{18}O$ = −7.5 - +3.4‰, $\delta^{17}O$ = −10.5‰ - +1.7‰), when applying a homogeneity threshold of ±0.45‰ (see Section 2.4), and 22 of 31 chondrules possess mean $\Delta^{17}O$ values between −6‰ and −4‰. The type II chondrule N16 shows a mean chondrule $\Delta^{17}O$ value of −2.28 ±0.15‰ (n = 4, 2SE); analysis of the BO chondrule N15 yields the highest mean $\Delta^{17}O$ value (−0.09 ±0.16‰, n = 10, 2SE). There is no apparent correlation of chondrule texture and mean chondrule oxygen isotope ratios.

## 4. Discussion

### 4.1. Parent body processes recorded in NWA 8613 and Kaba chondrules

The oxidized CV lithologies experienced extensive hydrous alteration that lead to the formation of secondary minerals in the chondrule mesostasis (e.g., Krot et al. 1995). Reduced CV chondrites were less affected by fluid-rock interactions, but were nonetheless subjected to various degrees of thermal metamorphism as described by Krot et al. (1995) or Kimura and Ikeda (1997). These differences in alteration style between oxidized and reduced CV lithologies can be also observed in chondrules of NWA 8613 and Kaba.

The degree of hydrous alteration experienced by chondrules in NWA 8613 ($CV3_{Red}$) is only mild compared to chondrules in Kaba ($CV3_{OxB}$), since phyllosilicates, often present in Kaba chondrules, are absent in chondrules of NWA 8613. However, plagioclase in mesostasis of NWA 8613 does show evidence for the presence of fluids; plagioclase oxygen isotopes are clearly distinguishable from those of olivine and pyroxene phenocrysts (Fig. 11a,b), i.e., plagioclase and phenocrysts are not in equilibrium in terms of oxygen isotopes. Similar observations were reported by Krot and Nagashima (2016) for plagioclase in Kaba and

related to re-equilibration of plagioclase with metasomatic fluids on the CV chondrite parent body. Data presented here on oxygen isotopes of plagioclase in Kaba, confirm these findings. Further, although data is limited, it appears that plagioclase in Kaba is more homogeneous regarding oxygen isotopes than plagioclase in NWA 8613 (Fig. 11b). Individual plagioclase analyses in chondrule N3 of NWA 8613, for instance, define a trend that - when extended - intersects the PCM line near to where the mean value of chondrule N3 plots (defined by olivine and pyroxene phenocrysts). This is interpreted as evidence for incomplete isotopic re-equilibration of these plagioclase crystals with asteroidal fluids. Moreover, more advanced oxygen isotope re-equilibration of plagioclase in Kaba chondrules is consistent with a more severe hydrous alteration of this chondrite compared to NWA 8613.

The degree of thermal metamorphism and aqueous alteration experienced by chondrites of petrologic type 3 can be assessed, for example, by studying the replacement of primary plagioclase by secondary minerals such as nepheline. Plagioclase grains selected for oxygen isotope analysis were determined to be free of nepheline lamellae based on careful backscattered electron imaging (see Section 2.3) of chondrules from both chondrites; EPMA analysis of these grains yield compositions that plot close to the ideal anorthite endmember composition on the anorthite-albite join (Fig. 4), demonstrating that nepheline formation was at most minor in the chondrules of NWA 8613 and Kaba that were surveyed in this study. Whereas all Kaba chondrules are visually free of nepheline, 4 of the 31 analyzed chondrules in NWA 8613 contain plagioclase with nepheline lamellae; EPMA analyses of those grains using a highly defocused beam (10 μm) are shifted towards the anorthite-nepheline join (Fig. 4).

Further, most chondrules in NWA 8613 contain olivine phenocrysts of variable FeO contents and mean Mg#'s of olivine are lower than those of corresponding pyroxenes (Fig. 5). This suggests that Mg-Fe diffusion during thermal metamorphism has altered pristine Mg#'s of olivine (Kimura and Ikeda 1997), whereas those of pyroxenes – in which diffusion rates are lower (e.g., Dohmen and Chakraborty 2007; Dohmen et al. 2016) – remain largely unaffected. This contrasts with findings from chondrites with lower petrologic grade ( $\leq$3.1) such as Acfer 094, CR chondrites, and also Kaba (Ushikubo et al. 2012; Tenner et al. 2015; Hertwig et al. 2018) in which Mg#'s of olivine and pyroxene are typically similar. Hence, to avoid underestimation, only pyroxene values were used in assigning mean Mg#'s to the chondrules of NWA 8613. Note that the overall nature of the pyroxenes present – such as no observed low-Ca pyroxene replacement and lack of any hedenbergite – is indicative of only mild thermal metamorphism.

### 4.2. Inferred dust enrichment and ice enhancement factors for chondrules in NWA 8613

This study reinforces the findings of previous investigations (Ushikubo et al. 2012; Tenner et al. 2013, 2015, 2017) which have shown that, when excluding isotopic relicts, olivine and low-Ca pyroxene phenocrysts as well as high-Ca pyroxene in chondrule mesostasis are indistinguishable in terms of $\Delta^{17}O$ values given analytical uncertainties (Fig. 10). Hence, during successive crystallization of chondrule phenocrysts and high-Ca pyroxenes, the isotopic composition of oxygen in the final chondrule melt did not change significantly. To

be clear, no systematic difference of $\Delta^{17}O$ values was observed among olivine, pyroxene, and high-Ca pyroxenes, which, if present, would be indicative of isotope exchange between ambient gas and a chondrule melt with distinct oxygen isotope ratios (e.g., Chaussidon et al. 2008; Marrocchi and Chaussidon 2015).

The curves of constant dust enrichments and ice enhancements shown in Figure 12 were calculated using the model of Tenner et al. (2015). The essence of this model is an oxygen isotope mass balance which considers Solar nebula gas, anhydrous silicate dust, water ice, and organics as oxygen reservoirs with distinctive $\Delta^{17}O$ values. Material originating from all of these reservoirs may become part of the chondrule precursor assemblage. Mean chondrule $\Delta^{17}O$ values are witnesses of mixing relations among them. For example, at constant dust enrichment but increasing ice enhancement factors, the mean $\Delta^{17}O$ values of chondrules increase and mean Mg#'s decrease due to the influence of the $^{16}O$-poor and oxidizing water ice reservoir. The model considers anhydrous silicate dust and water ice separately. The composition of the anhydrous silicate dust is calculated by treating all H in the dust of CI composition as part of the water ice (Tenner et al. 2015). Hence, only dust enrichment factors at an ice enhancement of 1x (the amount of ice in dust of CI composition) are directly comparable to those of other studies (e.g., Ebel and Grossman 2000).

For calculating the curves of constant dust enrichment and ice enhancements in Figure 12, effective $\Delta^{17}O$ values of the Solar nebula gas (−28.4‰) and organics in dust (+11.3‰) were adopted from Tenner et al. (2015); plausible $\Delta^{17}O$ values for the anhydrous silicate (−8‰) and water ice (+2‰) reservoirs in the CV chondrule-forming region were taken from Hertwig et al. (2018). The Mg#'s and $\Delta^{17}O$ values determined in this study for type I chondrules of NWA 8613 are consistent with moderate dust enrichment factors of between 50× and 150× CI dust relative to Solar abundances and with relatively dry conditions during chondrule formation (0.2-0.6× or up to 60% of the nominal ice in dust of CI composition). The BO chondrule N15 shows slightly higher values (~200× dust enrichment, 3× ice enhancement); formation of the only type II chondrule N16 would require dust enrichments >2000×. In comparison to NWA 8613, chondrules in Kaba tend to be more MgO-rich leading to slightly lower dust enrichment at similar ice enhancement factors (Fig. 12) (Hertwig et al. 2018). Estimated enrichment/enhancement factors are dependent on the assumed effective $\Delta^{17}O$ values of oxygen reservoirs, especially on the $\Delta^{17}O$ value of the anhydrous dust and water ice. However, as discussed by Tenner et al. (2015) and Hertwig et al. (2018), at moderately high dust enrichment factors (> ~50×), uncertainties in the effective $\Delta^{17}O$ value of anhydrous dust translate to only small differences in the estimated dust enrichment factors. Uncertainties in the isotope ratio of water ice, on the other hand, have a significant influence on ice enhancement factors, in such a way that, for instance, higher $\Delta^{17}O$ values cause lower estimated ice enhancements. These dust enrichment factors (~100× CI dust relative to gas of Solar composition) are within the range expected for turbulent protoplanetary disks (Cuzzi et al. 2001), but significantly higher than those estimated by Hubbard et al. (2018) (typically much smaller than 10×).

### 4.3. Comparison to CV and other carbonaceous chondrites

By comparing data sets from different CV and other carbonaceous chondrites, it is now possible to deduce general oxygen isotope characteristics of CV chondrules. The histogram in Figure 13a shows that most chondrules in the $CV_{red}$ chondrite NWA 8613 (27 of 31, or 87%) possess $\Delta^{17}O$ values ranging from −7‰ to −4‰. A similarily narrow range of chondrule $\Delta^{17}O$ values was also observed in the Kaba $CV_{oxB}$ (Hertwig et al. 2018) and in the Allende $CV_{oxA}$ (Rudraswami et al. 2011) chondrites as illustrated in the cumulative distribution plot of Figure 13b. Although Kaba contains a few chondrules with $\Delta^{17}O$ values below −7‰ (absent in NWA 8613), the distribution of chondrule $\Delta^{17}O$ values in both CV chondrites is almost identical (congruent distribution function in Fig. 13b). Around 60% of chondrules analyzed in Allende show $\Delta^{17}O$ values that fall between −6‰ to −5‰ and 81% of all chondrules possess values below −4‰ indicating the general prevalence of low $\Delta^{17}O$ values. The suite of CV chondrites shares the prevalence of MgO-rich (type I) chondrules with low $\Delta^{17}O$ values (< −4‰) with most other carbonaceous chondrites such as Yamato-81020 (CO, Tenner et al. 2013), Yamato-82094 (ungr. CC, Tenner et al. 2017), and Acfer 094 (ungr. CC, Ushikubo et al. 2012).

Varying proportions of type I chondrules in carbonaceous chondrites possess higher (e.g., ≥ −3‰) than typical $\Delta^{17}O$ values, while type II chondrules analyzed for oxygen isotopes are constantly $^{16}O$-poor (e.g., Schrader et al. 2014; Hertwig et al. 2018). In all carbonaceous chondrites but CR chondrites, type I chondrules with high $\Delta^{17}O$ values are subordinate. For example, in Allende, only 3 of in total 24 and in Yamato-81020 3 of 21 type I chondrules have $\Delta^{17}O$ values ≥−3‰ but the proportion of such $^{16}O$-poor type I chondrules is slightly higher in Acfer 094 (6 of 26). Conversely, NWA 8613 and Kaba don't contain type I chondrules with $\Delta^{17}O$ values ≥−3‰ which might be due to sampling bias. Type I chondrules with mean $\Delta^{17}O$ values < −4‰ are less abundant in the CR chondrites analyzed by Tenner et al. (2015) (25%, see Fig. 13b) and the bulk of chondrule $\Delta^{17}O$ values are within −3‰ and −1‰ (63%). In terms of the overall distribution of chondrule $\Delta^{17}O$ values, Acfer 094 occupies an intermediate position between CV and CR chondrites as indicated by the cumulative distribution pattern (Fig. 13b). The chondrule $\Delta^{17}O$ values form a bimodal distribution with 56% of chondrules (all type I) possessing $\Delta^{17}O$ values < −4‰.

The spread of $\Delta^{17}O$ values among type I chondrules can be attributed in large-part to the covariation of chondrule $\Delta^{17}O$ values and Mg#'s driven by different degrees of dust enrichment or ice enhancement (e.g., Connolly and Huss 2010; Tenner et al. 2015; Schrader et al. 2013, 2014; Hertwig et al. 2018). Although weakly developed, this covariation is also apparent for chondrules with low $\Delta^{17}O$ (< −4‰) and high Mg#'s in the NWA 8613 and Kaba CV chondrites (Fig. 12) and would hint to an increase in the amount of $^{16}O$-poor water ice in the precursor assemblage at constant and low (<200×) dust enrichments (Tenner et al. 2015; Hertwig et al. 2018).

### 4.4. Chondrules lying above the PCM and on the TF line

The NWA 8613-1 thin section contains one chondrule (N15, BO) with oxygen isotope ratios that plot on the TF line ($\Delta^{17}O$ ~ 0‰) and above the PCM line. Chondrules of similar isotopic composition are known from Yamato-82094 (Tenner et al. 2017), from CR

chondrites (Schrader et al. 2013), and from Acfer 094 (Ushikubo et al. 2012). Ferromagnesian minerals in this minor $^{16}$O-poor subpopulation of chondrules are moderately FeO-rich and chondrules occupy an intermediate position (between type I and type II compositions) in the Mg# distribution of their respective chondrites.

Mean isotope ratios of most chondrules of carbonaceous chondrites plot close to the PCM line which is a strong indication that the precursor reservoirs are also located along a slope-1 line (e.g., Tenner et al. 2015). In contrast, the $^{16}$O-poor chondrule subpopulation lie above this trend and, therefore, are likely genetically distinct from the bulk of other chondrules, i.e., at least one different precursor reservoir contributed to their formation (Clayton et al. 1983; Tenner et al. 2015). Tenner et al. (2017) proposed that the formation of $^{16}$O-poor chondrules with $\Delta^{17}O \sim 0‰$ (and above PCM line) observed in two CR chondrites possibly involved ordinary chondrite-like precursor material.

## 5. Conclusions

NWA 8613 is a newly described, unshocked $CV_{red}$ chondrite of low petrologic subtype (3.1-3.2) that experienced mild thermal metamorphism as indicated by, for instance, a limited amount of nepheline formation in chondrule mesostasis and moderate secondary FeO-zoning in olivine phenocrysts (Sato et al. 2016). The chondrules of NWA 8613 show porphyritic and barred textures and, as is typical for CV chondrites, are largely FeO-poor; only a single type II chondrule is present in the thin section.

The SIMS oxygen three-isotope analyses of chondrule olivine and pyroxene in NWA 8613 confirms findings of previous studies on different carbonaceous chondrites, including: (1) that individual mineral analyses plot on or close to the PCM line; and (2) that most chondrules are isotopically homogeneous in terms of the $\Delta^{17}$O values of chondrule olivine and pyroxenes. More specifically, each analyzed chondrule yielded at least four analytically indistinguishable oxygen isotope measurements, although approximately one third of these chondrules also contain $^{16}$O-rich or -poor isotopic relict olivine grains; forsteritic cores in the type II chondrule N16 are $^{16}$O-rich, dusty olivine in a porphyritic chondrule (N13) is $^{16}$O-poor relative to chondrule means.

Plagioclase in the chondrules of NWA 8613 and Kaba is $^{16}$O-poor relative to chondrule phenocrysts, indicating isotopic disequilibrium caused by aqueous alteration of plagioclase. Most plagioclase data from Kaba plot along a mass-dependent trend close to the TF line and are less variable than corresponding data from NWA 8613. In other words, observations are consistent with a higher degree of aqueous alteration of the Kaba chondrite.

The distribution of chondrule $\Delta^{17}$O values in NWA 8613 and Kaba are almost identical but potentially different from that in Allende. Oxygen three-isotope analyses of chondrules in these three CV chondrites demonstrate, however, that $\Delta^{17}$O values are predominately constrained to a narrow range between −6‰ and −4‰. The Mg#'s of pyroxenes (98.2 - 99.2) and mean $\Delta^{17}$O values (−6.66‰ - −3.55‰) of type I chondrules from NWA 8613 served as inputs for the oxygen isotope mass balance model of Tenner et al. (2015) that was slightly modified to account for possible differences in the oxygen isotope composition of

anhydrous silicate dust in the CR and CV chondrule-forming regions. Estimated dust enrichment and ice enhancement factors are low for type I chondrules (50× to 150× CI dust relative to Solar abundances, 0.2× to 0.6× nominal ice abundance in dust of CI composition). Findings agree with estimated values for chondrules in the Kaba CV chondrite, adding evidence in favor of a relatively dry and only moderately high dust-enriched disk in the CV chondrule-forming region.

## Supplementary Material

Refer to Web version on PubMed Central for supplementary material.

## Acknowledgments

The polished thin section of NWA 8613 used in this study was originally created by Mr. Sato and was later modified by Brian Hess to meet the dimensions and surface quality requirements of SIMS analysis. We thank the Smithonian Institution for providing the Kaba section. Dr. Akira Yamaguchi helped with phase analysis by EPMA at NIPR. We thank UW-Madison colleagues John Fournelle and Bill Schneider for assistance with SEM and EPMA work, Jim Kern and Mike Spicuzza for technical SIMS support, and Noël Chaumard for helpful discussions. We would like to thank the associate editor Alex Ruzicka and Emmanuel Jacquet for constructive reviews and Maciej G. Śliwiński for detailed language-related comments. WiscSIMS is partly supported by NSF (EAR-1658823). This work was supported by NASA (NNX14AG29G, NK) and by Grants-in-aid of Monkashou, Japan (No. 26400510 to MK).

## References

Baertschi P 1976 Absolute $^{18}O$ content of standard mean ocean water. Earth and Planetary Science Letters 31:341–344.

Berlin J, Jones RH, and Brearley AJ 2011 Fe-Mn systematics of type IIA chondrules in unequilibrated CO, CR, and ordinary chondrites. Meteoritics & Planetary Science 46(4):513–533.

Bonal L, Rouzaud J-N, and Quirico E 2006 Metamorphic Control of Noble Gas Abundances in Pristine Chondrites (abstract #1792). 37th Lunar and Planetary Science Conference.

Brearley AJ and Jones RH 1998 Chondritic Meteorites. Reviews in Mineralogy and Geochemistry 36:3–01–3–398.

Chaussidon M, Libourel G, and Krot AN 2008 Oxygen isotopic constraints on the origin of magnesian chondrules and on the gaseous reservoirs in the early Solar System. Geochimica et Cosmochimica Acta 72(7):1924–1938.

Clayton RN 1993 Oxygen Isotopes in Meteorites. Annual Review of Earth and Planetary Sciences 21(1):115–149.

Clayton RN 2008 Oxygen Isotopes in the Early Solar System - A Historical Perspective. Reviews in Mineralogy and Geochemistry 68(1):5–14.

Clayton RN, Onuma N, Grossman L, and Mayeda TK 1977 Distribution of the pre-Solar component in Allende and other carbonaceous chondrites. Earth and Planetary Science Letters 34:209–224.

Clayton RN, Onuma N, Ikeda Y, Mayeda TK, Hutcheon ID, Olsen EJ, and Molini-Velsko C 1983 Oxygen isotopic compositions of chondrules in Allende and ordinary chondrites In Chondrules and their origins, edited by King EA Huston, TX: Lunar and Planetary Institute pp. 37–43.

Connolly HC Jr. and Desch SJ 2004 On the origin of the “kleine Kügelchen” called Chondrules. Chemie der Erde - Geochemistry 64(2):95–125.

Connolly HC Jr. and Huss GR 2010 Compositional evolution of the protoplanetary disk: Oxygen isotopes of type-II chondrules from CR2 chondrites. Geochimica et Cosmochimica Acta 74(8):2473–2483.

Dohmen R, Becker H-W, and Chakraborty S 2007 Fe–Mg diffusion in olivine I: Experimental determination between 700 and 1,200°C as a function of composition, crystal orientation and oxygen fugacity. Physics and Chemistry of Minerals 34(6):389–407.

Dohmen R, Ter Heege JH, Becker H-W, and Chakraborty S 2016 Fe-Mg interdiffusion in orthopyroxene. American Mineralogist 101(10):2210–2221.

Donovan JJ 2015 Probe for EPMA v. 11.1.5: User's Guide and Reference. Eugene, OR: Probe Software, Inc. 429 p.

Ebel DS and Grossman L 2000 Condensation in dust-enriched systems. Geochimica et Cosmochimica Acta 64(2):339–366.

Frank DR, Zolensky ME, and Le L 2014 Olivine in terminal particles of Stardust aerogel tracks and analogous grains in chondrite matrix. Geochimica et Cosmochimica Acta 142:240–259.

Grossman JN 1988 Formation of chondrules In Meteorites and the Early Solar System, edited by Kerridge JF and Matthews MS Tucson: University of Arizona Press pp. 680–696.

Grossman JN and Brearley AJ 2005 The onset of metamorphism in ordinary and carbonaceous chondrites. Meteoritics & Planetary Science 40(1):87–122.

Hertwig AT, Defouilloy C, and Kita NT 2018 Formation of chondrules in a moderately high dust enriched disk: Evidence from oxygen isotopes of chondrules from the Kaba CV3 chondrite. Geochimica et Cosmochimica Acta 224:116–131. [PubMed: 30713348]

Hewins RH 1996 Chondrules and the protoplanetary disk: an overview In Chondrules and the protoplanetary disk, edited by Hewins RH, Jones RH, and Scott ERD Cambridge: Cambridge Univ. Press pp. 3–9.

Hubbard A, Mac Low M-M, Ebel DS 2018 Dust concentration and chondrule formation. Meteoritics & Planetary Science 53(7):1507–1515.

Jones RH 1996 FeO-rich, porphyritic pyroxene chondrules in unequilibrated ordinary chondrites. Geochimica et Cosmochimica Acta 60(16):3115–3138.

Keller LP and Buseck PR 1990 Aqueous alteration in the Kaba CV3 carbonaceous chondrite. Geochimica et Cosmochimica Acta 54:2113–2120.

Kimura M and Ikeda Y 1997 Anhydrous and aqueous alterations of Mokoia and Kaba CV3 chondrites. 22nd Symposium on Antarctic Meteorites, NIPR, Tokyo, 6 10–12, 1997. pp. 83–84.

Kimura M and Ikeda Y 1998 Hydrous and anhydrous alterations of chondrules in Kaba and Mokoia CV chondrites. Meteoritics & Planetary Science 33(5):1139–1146.

Kimura M, Barrat JA, Weisberg MK, Imae N, Yamaguchi A, and Kojima H 2014 Petrology and bulk chemistry of Yamato-82094, a new type of carbonaceous chondrite. Meteoritics & Planetary Science 49(3):346–357.

Kita NT and Ushikubo T 2012 Evolution of protoplanetary disk inferred from $^{26}$Al chronology of individual chondrules. Meteoritics & Planetary Science 47(7):1108–1119.

Kita NT, Huss GR, Tachibana S, Amelin Y, Nyquist LE, and Hutcheon ID 2005 Constraints on the Origin of Chondrules and CAIs from Short-lived and Long-lived Radionuclides In Chondrites and the protoplanetary disk, 1st ed., edited by Krot AN, Scott ERD, and Reipurth B San Francisco, CA: Astronomical Society of the Pacific pp. 558–587.

Kita NT, Nagahara H, Tachibana S, Tomomura S, Spicuzza MJ, Fournelle JH, and Valley JW 2010 High precision SIMS oxygen three isotope study of chondrules in LL3 chondrites: Role of ambient gas during chondrule formation. Geochimica et Cosmochimica Acta 74(22):6610–6635.

Kita NT, Defouilloy C, Kitajima K, Chaumard N, Hertwig A, Ishida A, and Valley JW 2017 Analytical development for SIMS high precision oxygen and magnesium isotope analyses of meteoritic and cometary samples (abstract #1754). 48th Lunar and Planetary Science Conference.

Kleine T and Rudge JF 2011 Chronometry of Meteorites and the Formation of the Earth and Moon. Elements 7(1):41–46.

Krot AN and Nagashima K 2016 Evidence for Oxygen-Isotope Exchange in Chondrules and Refractory Inclusions During Fluid-Rock Interaction on the CV Chondrite Parent Body (abstract #6014). Meteoritics and Planetary Science Supplement 51:A249.

Krot AN, Scott ERD, and Zolensky ME 1995 Mineralogical and chemical modification of components in CV3 chondrites: Nebular or asteroidal processing? Meteoritics & Planetary Science 30:748–775.

Krot AN, Petaev MI, Scott ERD, Choi B-G, Zolensky ME, and Keil K 1998 Progressive alteration in CV3 chondrites: More evidence for asteroidal alteration. Meteoritics & Planetary Science 33:1065–1085.

Krot AN, Fegley B, Lodders K, and Palme H 2000 Meteoritical and astrophysical constraints on the oxidation state of the Solar nebula In Protostars and Planets IV, edited by Mannings V, Boss AP, and Russell SS Tucson: University of Arizona Press pp. 1019–1054.

Krot AN, Yurimoto H, McKeegan KD, Leshin LA, Chaussidon M, Libourel G, Yoshitake M, Huss GR, Guan Y, and Zanda B 2006 Oxygen isotopic compositions of chondrules: Implications for evolution of oxygen isotopic reservoirs in the inner solar nebula. Chemie der Erde - Geochemistry 66(4):249–276.

Krot AN, Amelin Y, Bland P, Ciesla FJ, Connelly J, Davis AM, Huss GR, Hutcheon ID, Makide K, Nagashima K, Nyquist LE, Russell SS, Scott ERD, Thrane K, Yurimoto H, and Yin Q-Z 2009 Origin and chronology of chondritic components: A review. Geochimica et Cosmochimica Acta 73(17):4963–4997.

Kunihiro T, Rubin AE, McKeegan KD, and Wasson JT 2004 Oxygen-isotopic compositions of relict and host grains in chondrules in the Yamato 81020 CO3.0 chondrite. Geochimica et Cosmochimica Acta 68(17):3599–3606.

Kunihiro T, Rubin AE, and Wasson JT 2005 Oxygen-isotopic compositions of low-FeO relicts in high-FeO host chondrules in Acfer 094, a type 3.0 carbonaceous chondrite closely related to CM. Geochimica et Cosmochimica Acta 69(15):3831–3840.

Libourel G and Chaussidon M 2011 Oxygen isotopic constraints on the origin of Mg-rich olivines from chondritic meteorites. Earth and Planetary Science Letters 301(1–2):9–21.

Marrocchi Y and Chaussidon M 2015 A systematic for oxygen isotopic variation in meteoritic chondrules. Earth and Planetary Science Letters 430:308–315.

McSween H 1977 Petrographic variations among carbonaceous chondrites of the Vigarano type. Geochimica et Cosmochimica Acta 41:1777–1790.

Nagahara H 1981 Evidence for secondary origin of chondrules. Nature 292:135–136.

Nakashima D, Kita NT, Ushikubo T, Noguchi T, Nakamura T, and Valley JW 2013 Oxygen three-isotope ratios of silicate particles returned from asteroid Itokawa by the Hayabusa spacecraft: A strong link with equilibrated LL chondrites. Earth and Planetary Science Letters 379:127–136.

Rubin AE 2000 Petrologic, geochemical and experimental constraints on models of chondrule formation. Earth-Science Reviews 50(1–2):3–27.

Rudraswami NG, Ushikubo T, Nakashima D, and Kita NT 2011 Oxygen isotope systematics of chondrules in the Allende CV3 chondrite: High precision ion microprobe studies. Geochimica et Cosmochimica Acta 75(23):7596–7611.

Ruzicka A, Hiyagon H, Hutson M, Floss C 2007 Relict olivine, chondrule recycling, and the evolution of nebular oxygen reservoirs. Earth and Planetary Science Letters 257:274–289.

Ruzicka A, Grossman J, Bouvier A, and Agee CB 2017 The Meteoritical Bulletin, No. 103. Meteoritics & Planetary Science 52(5):1014.

Sato R, Kimura M, and Fujiya W 2016 A primitive chondrite, NWA 8613 chondrite, CV3.1–3.2. Japan Geoscience Meeting:PPS12–P07.

Schrader DL, Connolly HC Jr., Lauretta DS, Nagashima K, Huss GR, Davidson J, and Domanik KJ 2013 The formation and alteration of the Renazzo-like carbonaceous chondrites II: Linking O-isotope composition and oxidation state of chondrule olivine. Geochimica et Cosmochimica Acta 101:302–327.

Schrader DL, Nagashima K, Krot AN, Ogliore RC, and Hellebrand E 2014 Variations in the O-isotope composition of gas during the formation of chondrules from the CR chondrites. Geochimica et Cosmochimica Acta 132:50–74.

Scott ERD and Krot AN 2007 1.07 - Chondrites and their components In Treatise on Geochemistry, Volume 1: Meteorites, Comets, and Planets, edited by Holland HF and Turekian KK Amsterdam, San Francisco, CA: Elsevier pp. 1–72.

Tenner TJ, Ushikubo T, Kurahashi E, Kita NT, and Nagahara H 2013 Oxygen isotope systematics of chondrule phenocrysts from the CO3.0 chondrite Yamato 81020: Evidence for two distinct oxygen isotope reservoirs. Geochimica et Cosmochimica Acta 102:226–245.

Tenner TJ, Nakashima D, Ushikubo T, Kita NT, and Weisberg MK 2015 Oxygen isotope ratios of FeO-poor chondrules in CR3 chondrites: Influence of dust enrichment and $H_2O$ during chondrule formation. Geochimica et Cosmochimica Acta 148:228–250.

Tenner TJ, Kimura M, and Kita NT 2017 Oxygen isotope characteristics of chondrules from the Yamato-82094 ungrouped carbonaceous chondrite: Further evidence for common O-isotope environments sampled among carbonaceous chondrites. Meteoritics & Planetary Science 52(2):268–294.

Ushikubo T, Kimura M, Kita NT, and Valley JW 2012 Primordial oxygen isotope reservoirs of the solar nebula recorded in chondrules in Acfer 094 carbonaceous chondrite. Geochimica et Cosmochimica Acta 90:242–264.

Valley JW and Kita NT 2009 In situ oxygen isotope geochemistry by ion microprobe In Secondary Ion Mass Spectrometry in the Earth Sciences, edited by Fayek M Mineralogical Society of Canada pp. 19–63.

Villeneuve J, Chaussidon M, and Libourel G 2009 Homogeneous Distribution of $^{26}$Al in the Solar System from the Mg Isotopic Composition of Chondrules. Science 325(5943):985–988. [PubMed: 19696348]

Wasson JT and Rubin AE 2003 Ubiquitous low-FeO relict grains in type II chondrules and limited overgrowths on phenocrysts following the final melting event. Geochimica et Cosmochimica Acta 67(12):2239–2250.

Weisberg MK, Prinz M, Clayton RN, and Mayeda TK 1997 CV3 chondrites: Three subgroups, not two. Meteoritics & Planetary Science 32:A138–139.

Young ED and Russell SS 1998 Oxygen Reservoirs in the Early Solar Nebula Inferred from an Allende CAI. Science 282:452–455.

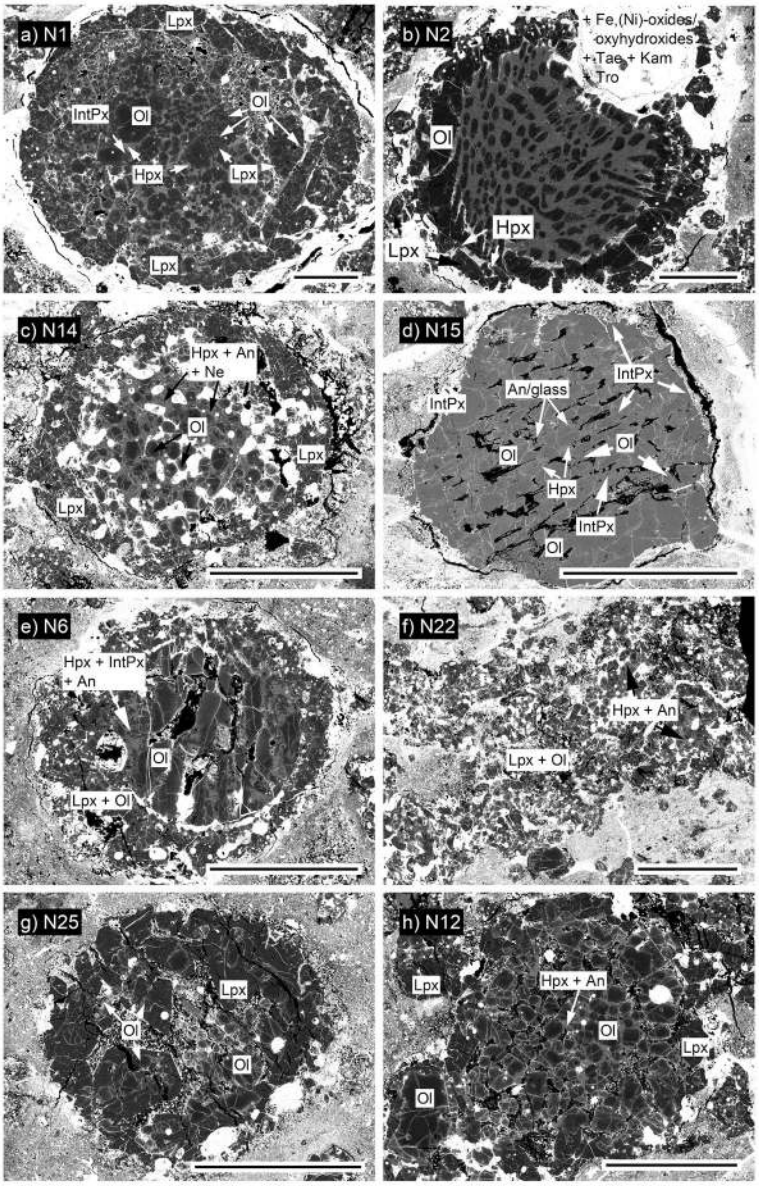


**Fig. 1.**

BSE imagery showing the range of chondrule textures encountered in thin section of NWA 8613. (a) N1: large POP chondrule encased by shell of coarse-grained low-Ca pyroxene laths. (b) N2: BO chondrule partially encased by a low-Ca pyroxene shell. The embedded BSE-bright sphere comprises various opaque phases (c) N14 (POP): kamacite/taenite and Fe-sulfides located in between PO interior and low-Ca pyroxene shell as well as in the chondrule center. (d) N15: BO chondrule in which relatively Fe-rich olivine (Mg# ~ 90) occurs alongside intermediate and high-Ca pyroxene. (e) N6: POP chondrule with spherical olivine-rich interior enclosed in low-Ca pyroxene- and olivine-rich shell. (f) N22 (POP): amoeboid-shaped chondrule rich in opaque phases. The small enclaves of mesostasis are composed of high-Ca pyroxene and anorthite. (g) N25: POP chondrule with coarse grained and euhedral low-Ca pyroxenes. (h) N12 (POP): center of chondrule is composed of

granular olivine encased by partial shell of low-Ca pyroxene. Scale bar in all panels: 500 μm. Ol: olivine, Lpx: low-Ca pyroxene, Hpx: high-Ca pyroxene, IntPx: intermediate pyroxene, An: anorthitic plagioclase, Ne: nepheline, Tae: taenite, Kam: kamacite, Tro: troilite.

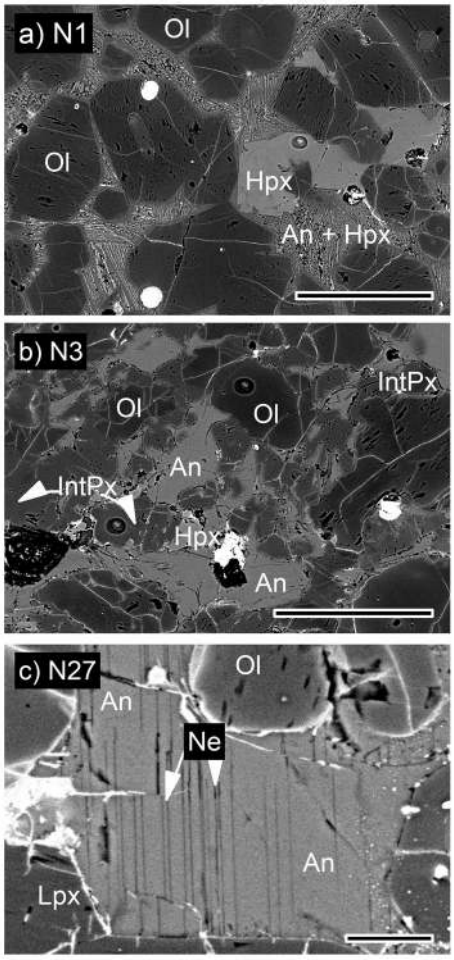


**Fig. 2.**

BSE imagery showing three typical mesostasis textures. Chondrule mesostasis can comprise (a) subhedral to euhedral high-Ca pyroxene crystals (± intermediate pyroxenes) embedded in plagioclase containing high-Ca pyroxene dendrites, and (b) intermediate and high-Ca pyroxenes as well as anorthitic plagioclase. (c) Anorthitic plagioclase sometimes contains small nepheline lamellae. Scale bar in a) and b): 100 μm, c): 10 μm. Ol: olivine, Lpx: low-Ca pyroxene, Hpx: high-Ca pyroxene, IntPx: intermediate pyroxene, An: anorthitic plagioclase, Ne: nepheline.

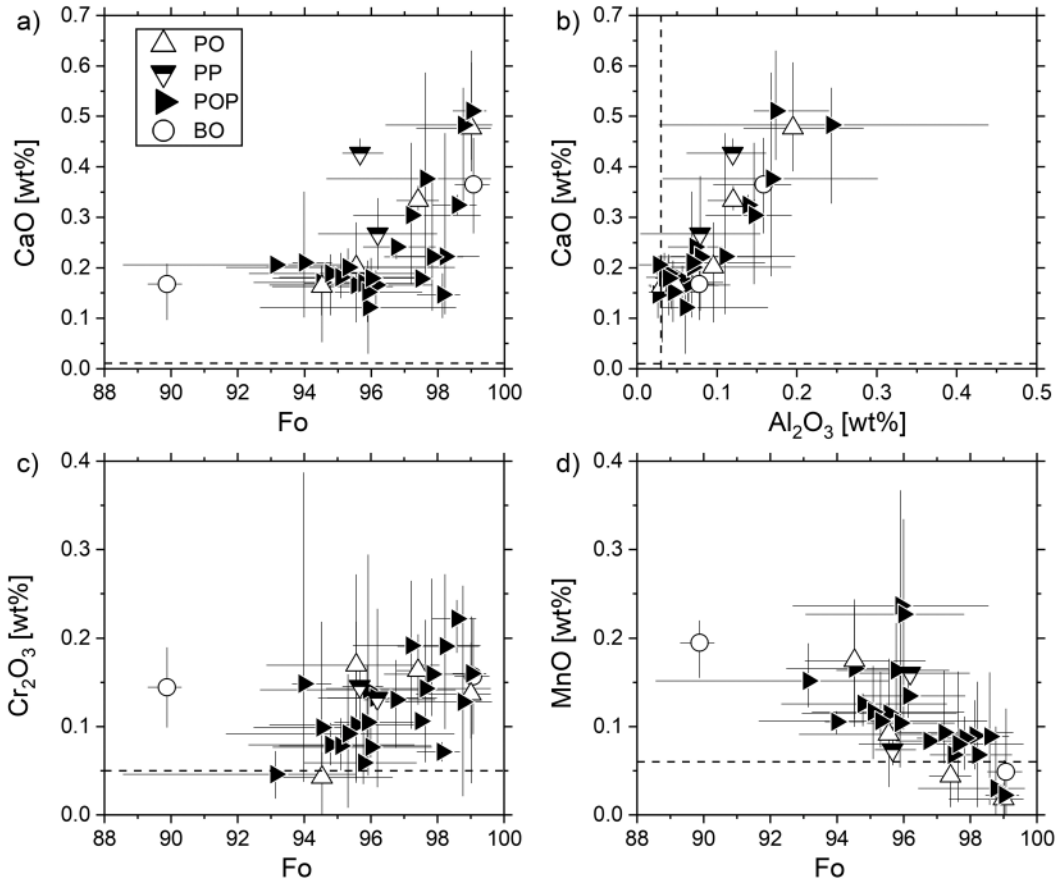


**Fig. 3.**

Plots showing compositional trends among the minor elements hosted by the same olivine and pyroxene phenocrysts in chondrules of NWA 8613 for which oxygen three-isotope ratios were determined in this study (type I only). Chondrule olivine of higher Fo content tends to be: (a) richer in CaO and (b) higher CaO contents in turn correlate with elevated $Al_2O_3$ concentrations. (c) Measured $Cr_2O_3$ in olivine loosely correlates with Fo content. (d) Mean MnO contents are below or close to the mean detection limit for high-Mg# chondrules. Data points represent chondrule means and error bars show full range of measured values. Dashed lines indicate mean detection limits (3σ).

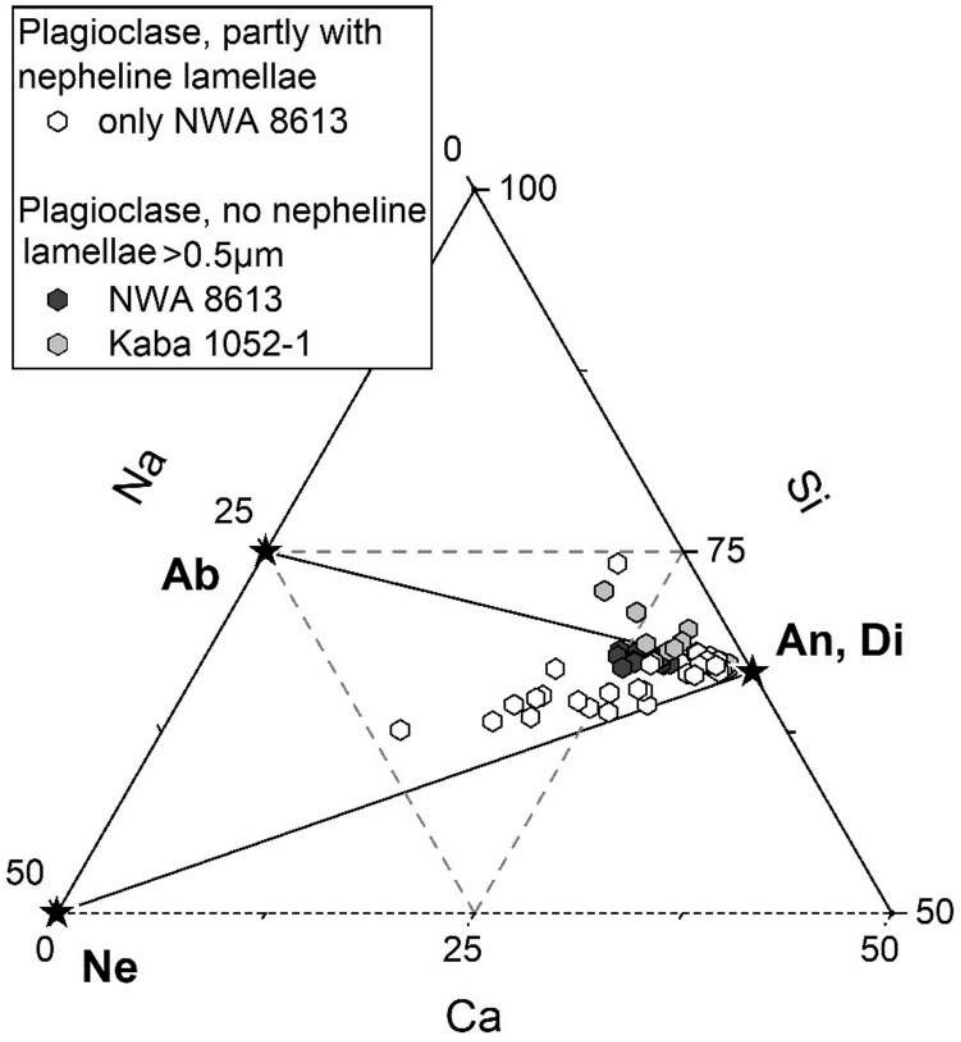


**Fig. 4.**

Ternary compositional diagram showing molar proportions of Ca, Na, and Si in two different sets of plagioclase EPMA measurements. Plagioclase showing >1 μm wide nepheline lamellae (open symbols; analyzed using 10 μm electron beam) is shifted towards nepheline (Ne) endmember composition, whereas plagioclase without visible nepheline plots close to the anorthite (An)- albite (Ab) join. Analyses of the last dataset were used for correcting instrumental bias of plagioclase SIMS analyses (see Data S4).

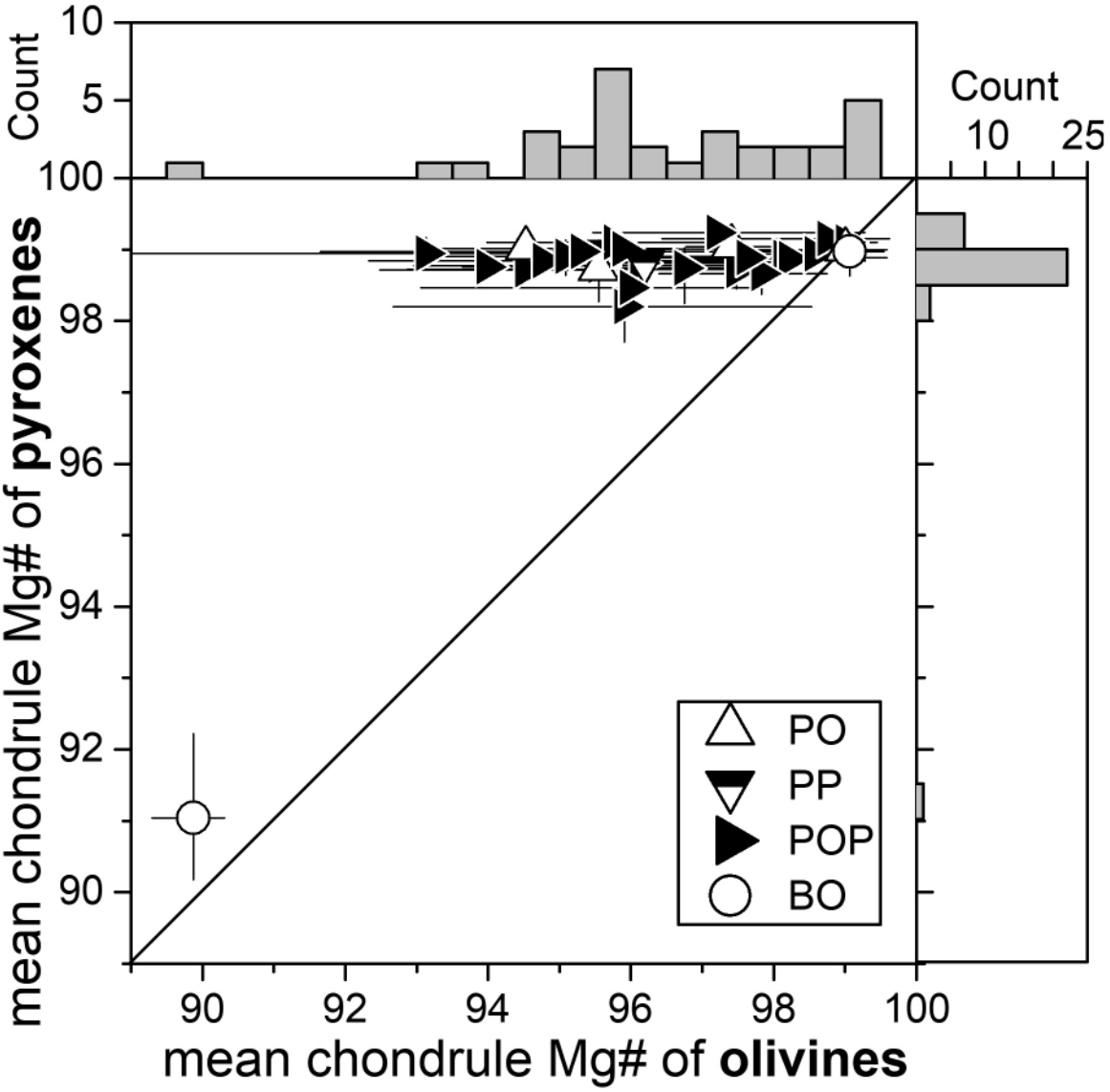


**Fig. 5.**

Mean Mg# of pyroxenes vs. mean Mg# of olivine of individual chondrules. With the exception of chondrule N15, mean chondrule Mg#'s of pyroxenes are consistently higher than 98 while those of olivine show a range of mostly lower values (Mg#: 93 - 99).

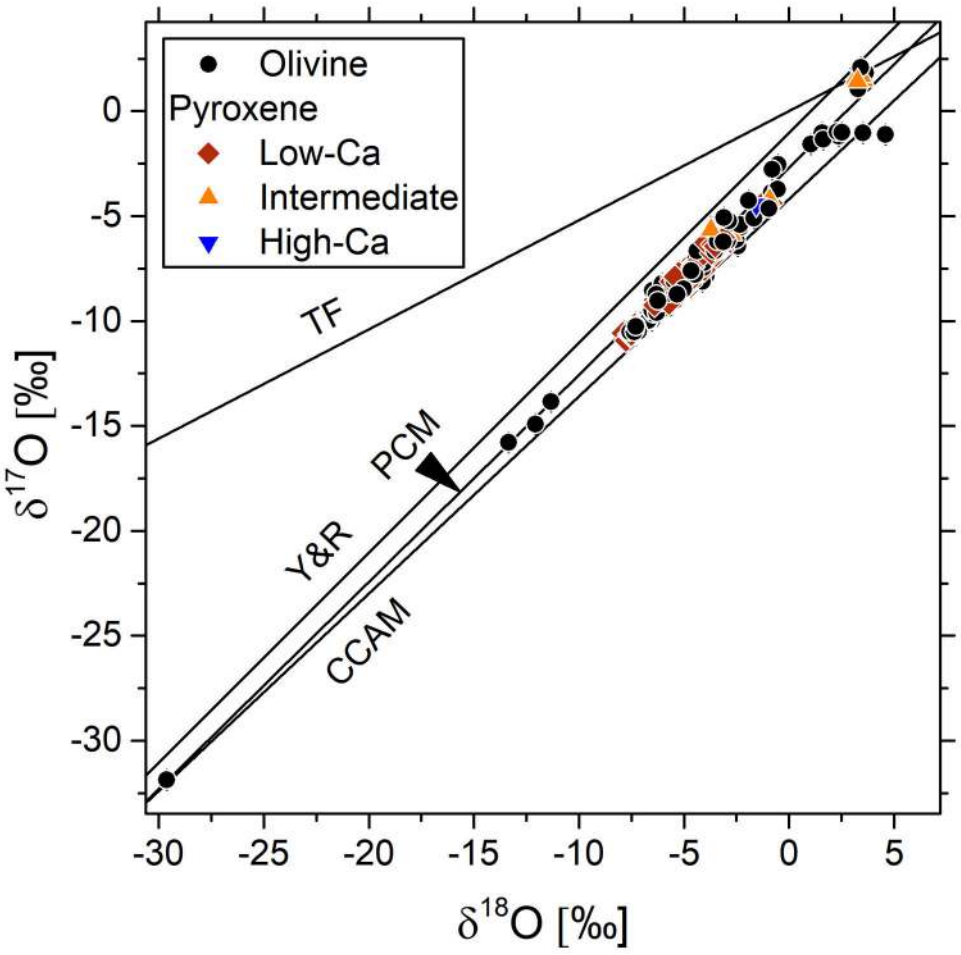


**Fig. 6.**

Oxygen three-isotope ratios of olivine and pyroxene (n=262) measured in chondrules of NWA 8613. Most analyses plot along the PCM line (Ushikubo et al. 2012), close to the CCAM line (Clayton et al. 1977); notable exceptions are olivine and pyroxene analyses of chondrule N15 which plot on the TF (terrestrial fractionation) line and two olivine analyses from the type II chondrule N16 that are fractionated towards higher $\delta^{18}O$ values. Y&R: Young & Russel line (Young and Russell 1998).

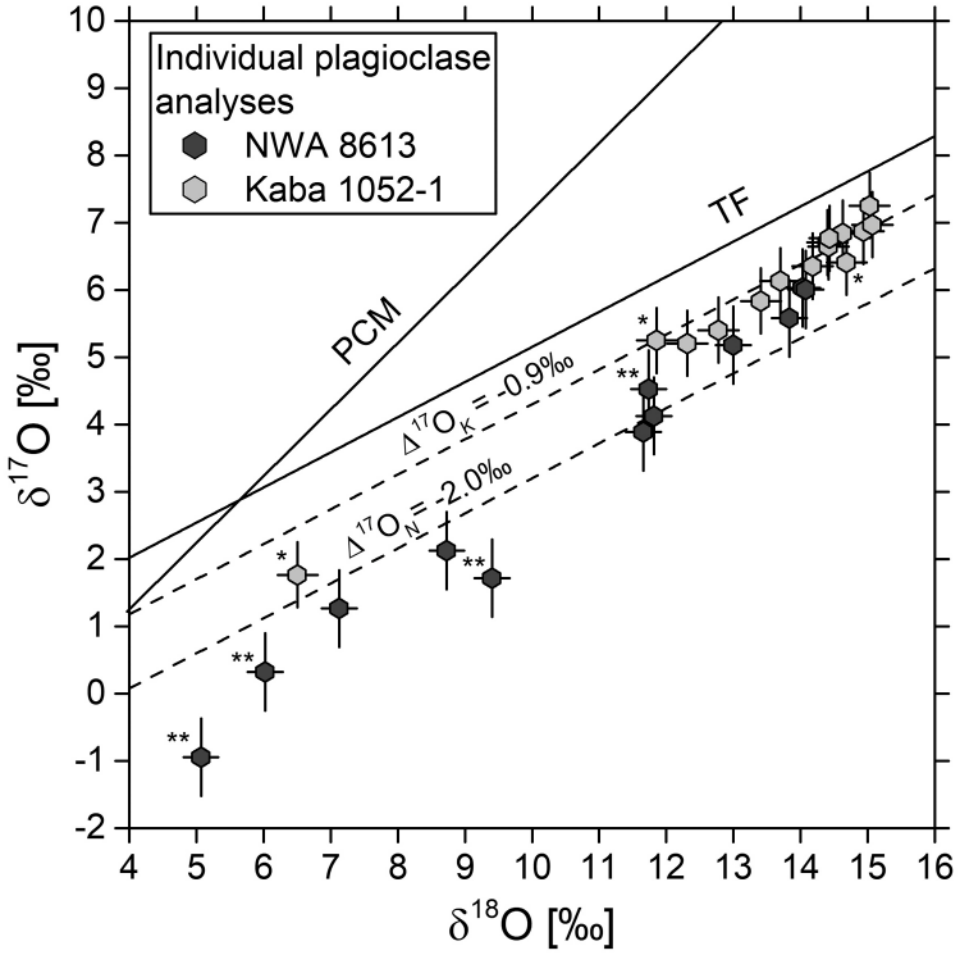


**Fig. 7.**

Oxygen three-isotope ratios of plagioclase analyzed in chondrules of NWA 8613 and Kaba. Analyses of plagioclase in Kaba follow a mass-dependent trend characterized by a $\Delta^{17}O_K$ value of −0.9‰. Plagioclase in NWA 8613 is more variable; average $\Delta^{17}O_N$ value = −2.0 ‰. Most of the spread along the $\delta^{18}O$ axis is introduced by plagioclase data from only two chondrules (* K1; ** N3).

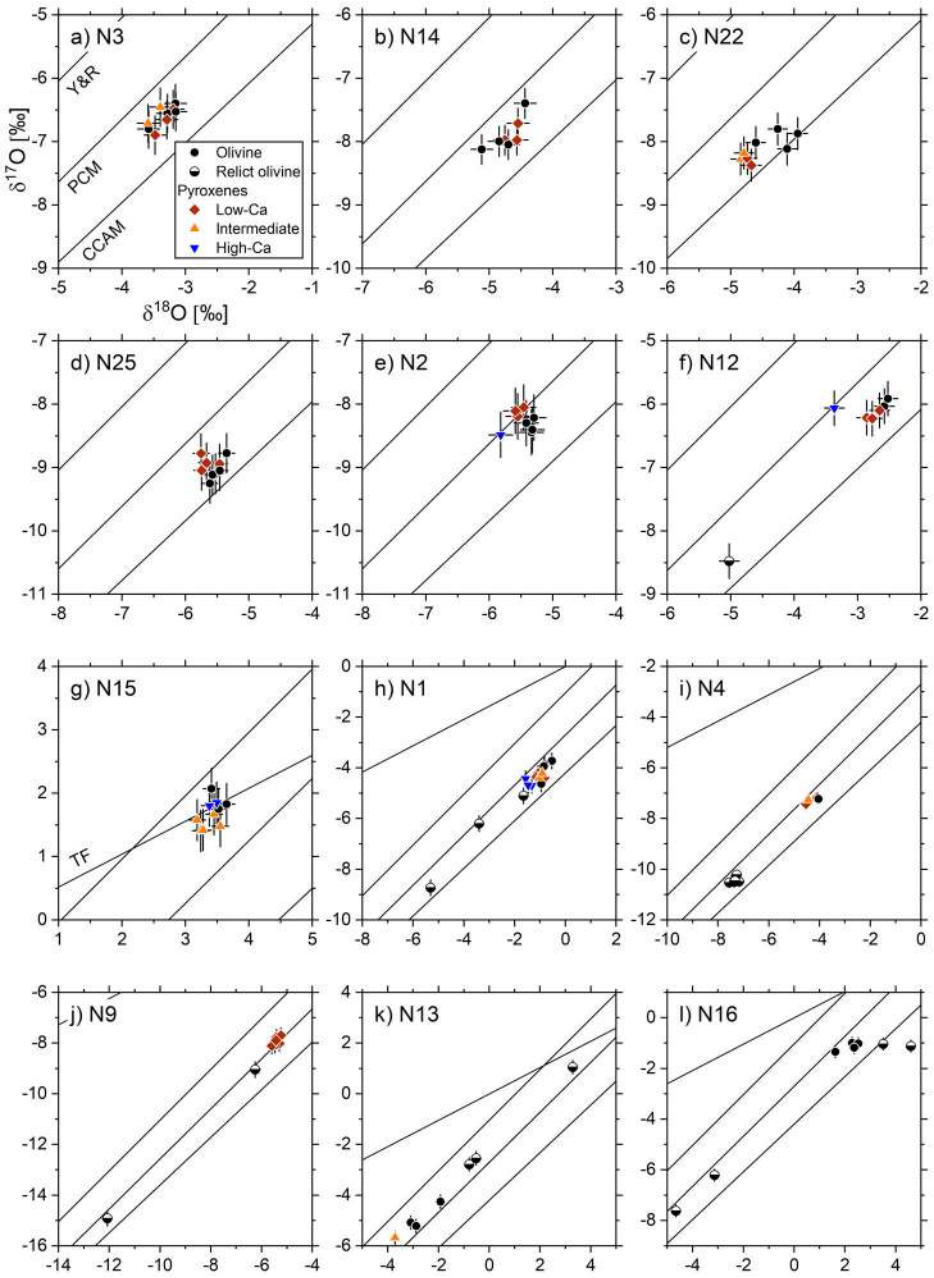


**Fig. 8:**

Oxygen three-isotope diagrams displaying olivine and pyroxene analyses of individual chondrules. Error bars represent the external reproducibility (2SD) of SIMS measurements as defined by analyses of a bracketing standard. (a-d) Chondrules are internally homogeneous in terms of the $\Delta^{17}O$ values of analyzed minerals and the relevant homogeneity criteria (see Section 2.4.). (e-g) High-Ca and intermediate pyroxenes are indistinguishable from low-Ca pyroxene and olivine in respect to $\Delta^{17}O$. (h-l) Isotopic relict olivine is $^{16}O$-rich or $^{16}O$-poor relative to analyses that define the mean chondrule isotope ratios. Two olivine analyses in the type II chondrule N16 are fractionated in the direction of higher $\delta^{18}O$ values. See Fig. 6 for references for the PCM, CCAM, Y&R, and TF lines.

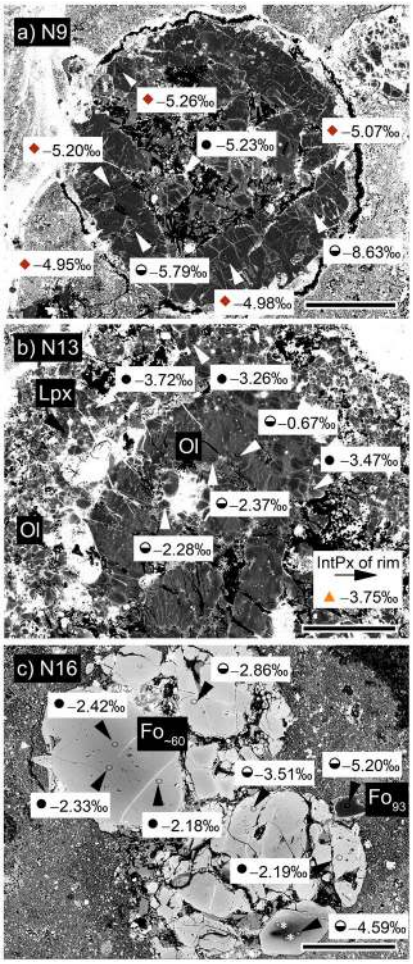


**Fig. 9.**

BSE images of a selection of chondrules containing isotopic relict olivine. (a) SIMS analysis of olivine inclusions in chondrule N9 yielded $^{16}$O-rich compositions relative to those of enclosing low-Ca pyroxene laths and another olivine grains. (b) Chondrule N13 contains $^{16}$O-poor dusty olivine relicts that are distinct from olivine and pyroxene of the chondrule rim. (c) Forsteritic cores are $^{16}$O-rich in comparison with fayalitic olivine in the type II PO chondrule fragment. Legend symbols as in Fig. 8. (*) Location of SIMS measurements with no corresponding EPMA analyses. Scale bar is 200 μm for (a) and (b), 150 μm for (c).

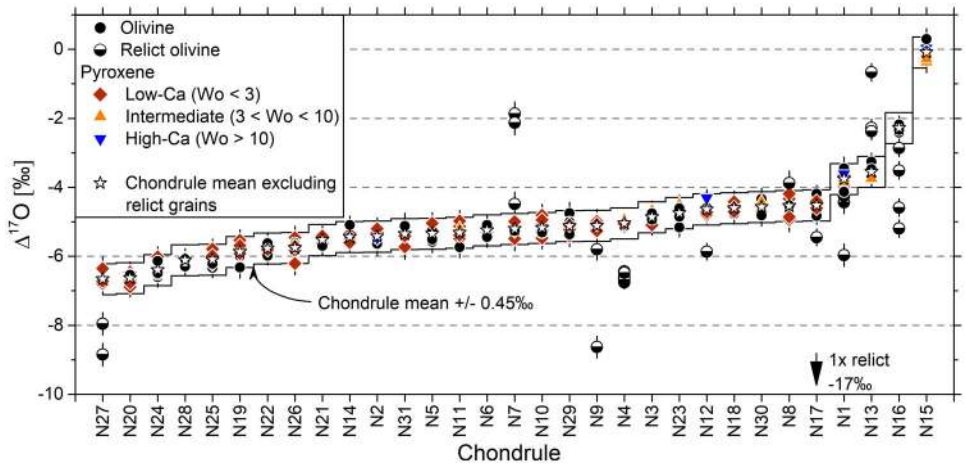


**Fig. 10.**

Summary plot showing $\Delta^{17}O$ values of individual olivine and pyroxene analyses, grouped by chondrule and ordered according to increasing chondrule means (stars). In 21 of the 31 chondrules, no isotopic relict olivine was observed. All chondrules contain at least 4 pyroxene/olivine analyses that are isotopically ($\Delta^{17}O$) homogeneous considering a threshold of ±0.45‰ from the mean. Mean chondrule $\Delta^{17}O$ values range from approximately −7‰ to 0‰.

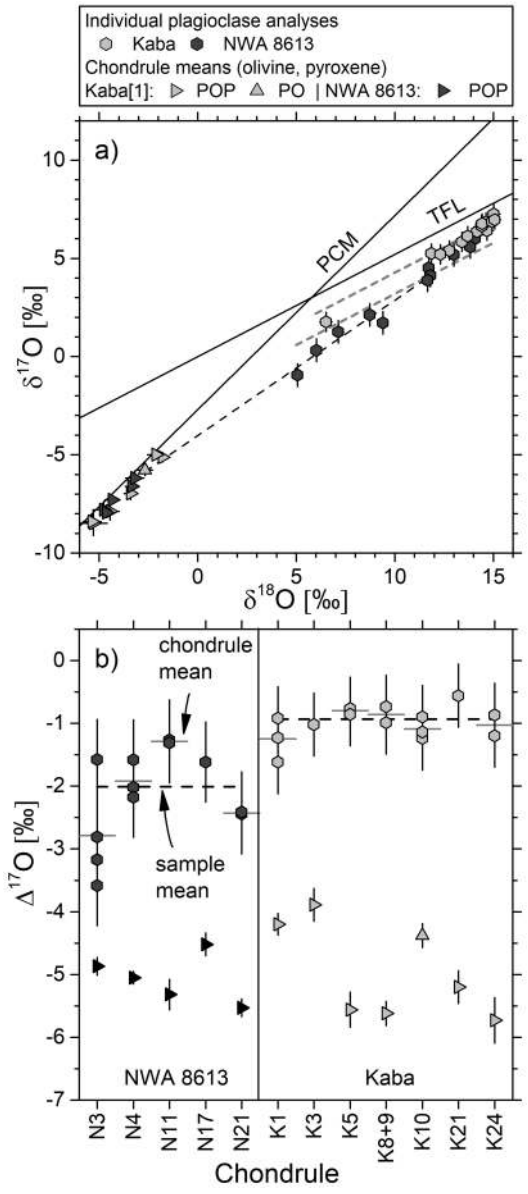


**Fig. 11.**

Oxygen isotope ratios of individual plagioclase analyses and mean chondrule oxygen isotope ratios of NWA 8613 and Kaba (only those chondrule means with plagioclase analyses are shown). (a) Mean chondrule isotope ratios follow a mass-independent trend (PCM line) whereas plagioclase analyses line up (sub)parallel to the TF line; dashed lines parallel to TF line symbolize sample means (see Fig. 7). Extension of the linear trend through plagioclase of chondrule N3 (NWA 8613) intersects the PCM line near the mean value of this chondrule. (b) $\Delta^{17}O$ values of plagioclase are independent of corresponding mean chondrule $\Delta^{17}O$ values. Plagioclase analyses of NWA 8613 are less homogeneous than those of Kaba. [1] mean chondrule $\Delta^{17}O$ values of Kaba are from Hertwig et al. (2018).

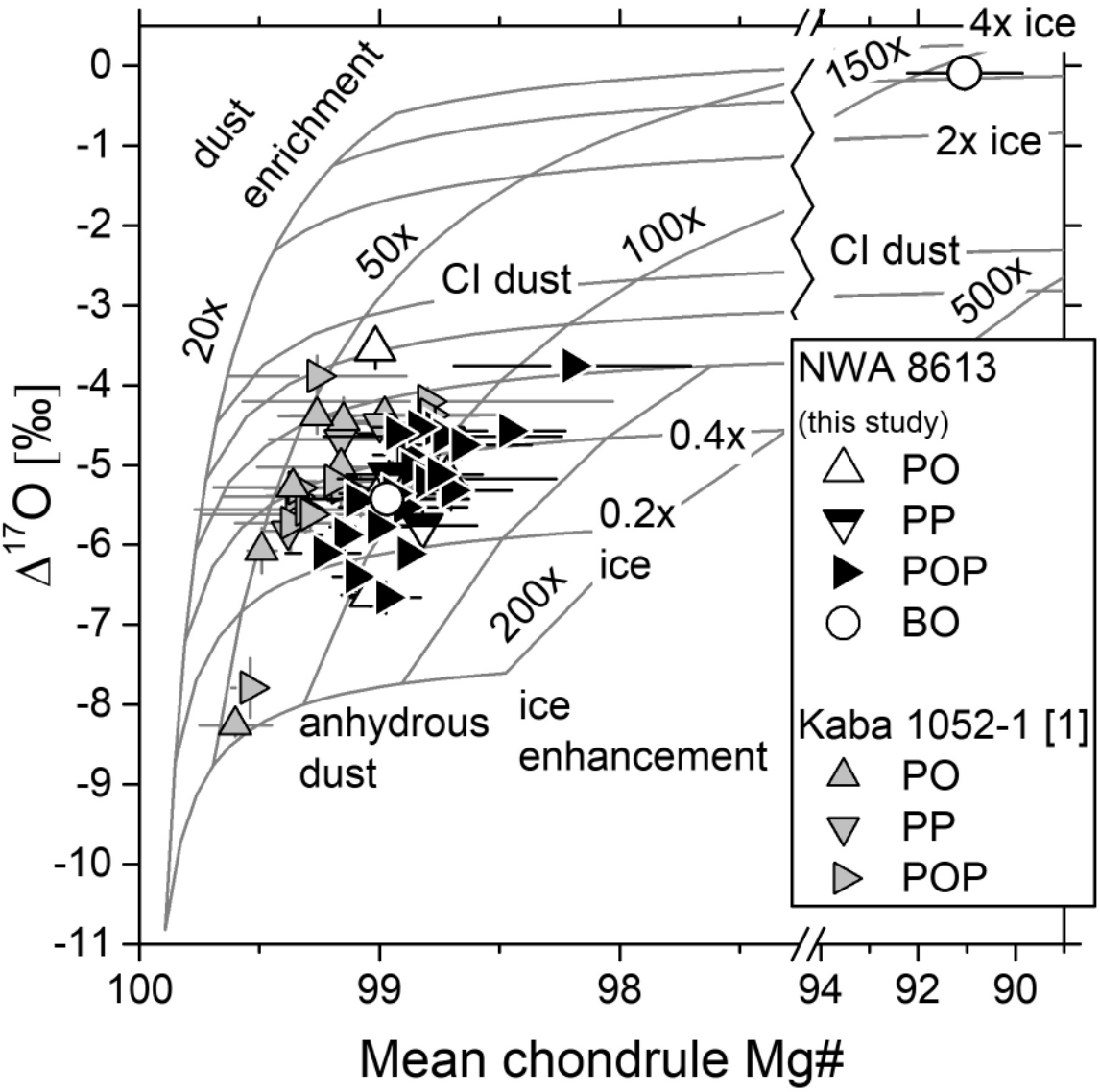


**Fig. 12.**

Mean chondrule $\Delta^{17}O$ values plotted against mean Mg#'s of type I chondrules in NWA 8613 (only Mg#'s of pyroxenes) and Kaba ([1], Hertwig et al. 2018). Note that Mg#'s of chondrule olivine and pyroxenes in Kaba are indistinguishable for each chondrule. Superimposed are curves of constant dust enrichment and ice enhancement calculated with model of Tenner et al. (2015), assuming the $\Delta^{17}O$ value of anhydrous silicate dust to be −8‰ and that of water ice to be +2‰ (Hertwig et al. 2018). $\Delta^{17}O$ values and Mg#'s reflect relatively dry (~ 0.2×–0.6× nominal ice in CI dust) conditions during chondrule formation for both CV chondrites and low (50-150× CI dust relative to Solar abundances) dust enrichments.

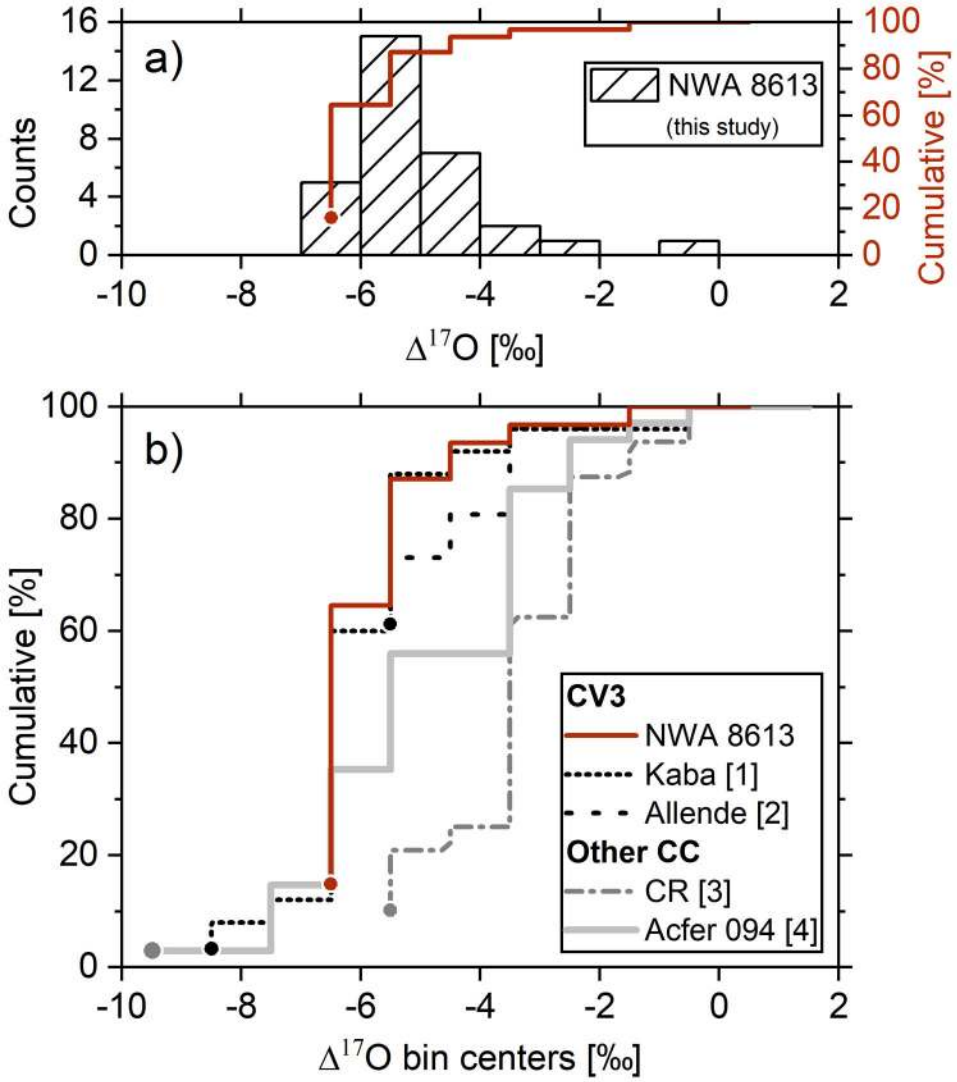


**Fig. 13.**

Histogram of mean chondrule $\Delta^{17}O$ values of NWA 8613 and cumulative distribution plot of $\Delta^{17}O$ values of various carbonaceous chondrites. (a) 27 of 31 or 87% of all chondrules in NWA 8613 have mean $\Delta^{17}O$ values in between −7‰ and −4‰. (5 of 31 or 16% of chondrules possess $\Delta^{17}O$ values between −7‰ and −6‰). b) Distribution of mean $\Delta^{17}O$ values in CV ([1], Hertwig et al. 2018; [2], Rudraswami et al. 2011) and other carbonaceous chondrites ([3], Tenner et al. 2015; [4], Ushikubo et al. 2012) compared to that in NWA 8613. The distributions of chondrule $\Delta^{17}O$ values in Kaba and NWA 8613 are nearly identical.

**Table 1.**

Oxygen isotope ratios and chemical composition (mol.% anorthite endmember) of plagioclase in NWA 8613 and Kaba. Mean $\Delta^{17}O$ values of plagioclase per chondrite are calculated based on chondrule means.

| Ch# | Analysis | An | $\delta^{17}O$ | 2SD[a] | $\delta^{18}O$ | 2SD[a] | $\Delta^{17}O$ | 2SD[a] | $\Delta^{17}O$ mean | 2SD[b] | An mean |
|---|---|---|---|---|---|---|---|---|---|---|---|
| *Kaba 1052-1* | | | | | | | | | | | |
| K1 | K1: 19.pl | 91 | 6.41 | 0.48 | 14.69 | 0.30 | −1.23 | 0.50 | −1.25 | 0.70 | 83 |
| | K1: 21.pl | 78 | 1.77 | 0.48 | 6.51 | 0.30 | −1.62 | 0.50 | | | |
| | K1: 22.pl | 81 | 5.25 | 0.48 | 11.86 | 0.30 | −0.92 | 0.50 | | | |
| K3 | K3: 23.pl | 91 | 6.35 | 0.48 | 14.18 | 0.30 | −1.02 | 0.50 | −1.02 | | |
| K5 | K5: 24.pl | 95 | 6.71 | 0.48 | 14.40 | 0.30 | −0.78 | 0.50 | −0.80 | 0.10 | 94 |
| | K5: 25.pl | 95 | 6.84 | 0.48 | 14.63 | 0.30 | −0.76 | 0.50 | | | |
| | K5: 26.pl | 91 | 6.64 | 0.48 | 14.42 | 0.30 | −0.85 | 0.50 | | | |
| K8+9 | K8+9: 28.pl | 94 | 6.77 | 0.48 | 14.43 | 0.30 | −0.73 | 0.50 | −0.86 | 0.36 | 95 |
| | K8+9: 30.pl | 96 | 6.13 | 0.48 | 13.70 | 0.30 | −0.99 | 0.50 | | | |
| K10 | K10: 31.pl | 96 | 5.84 | 0.48 | 13.41 | 0.30 | −1.14 | 0.50 | −1.09 | 0.35 | 93 |
| | K10: 32.pl | 92 | 5.40 | 0.48 | 12.78 | 0.30 | −1.24 | 0.50 | | | |
| | K10: 33.pl | 92 | 6.87 | 0.48 | 14.94 | 0.30 | −0.90 | 0.50 | | | |
| K21 | K21: 34.pl | 83 | 7.25 | 0.48 | 15.03 | 0.30 | −0.56 | 0.50 | −0.56 | | |
| K24 | K24: 35.pl | 87 | 6.97 | 0.48 | 15.07 | 0.30 | −0.86 | 0.50 | −1.03 | 0.47 | 86 |
| | K24: 36.pl | 85 | 5.21 | 0.48 | 12.31 | 0.30 | −1.20 | 0.50 | | | |
| | | | | | | | sample mean: | | −0.94 | 0.45 | |
| *NWA 8613* | | | | | | | | | | | |
| N3 | N3: 41.pl | 83 | −0.95 | 0.57 | 5.07 | 0.26 | −3.58 | 0.64 | −2.79 | 1.73 | 84 |
| | N3: 42.pl | 83 | 1.72 | 0.57 | 9.41 | 0.26 | −3.17 | 0.64 | | | |
| | N3: 43.pl | 84 | 0.32 | 0.57 | 6.03 | 0.26 | −2.81 | 0.64 | | | |
| | N3: 44.pl | 84 | 4.53 | 0.57 | 11.74 | 0.26 | −1.57 | 0.64 | | | |
| N4 | N4: 45.pl | 78 | 4.13 | 0.57 | 11.82 | 0.26 | −2.02 | 0.64 | −1.92 | 0.62 | 78 |
| | N4: 46.pl | 77 | 5.18 | 0.57 | 13.00 | 0.26 | −1.58 | 0.64 | | | |
| | N4: 47.pl | 79 | 3.89 | 0.57 | 11.66 | 0.26 | −2.18 | 0.64 | | | |
| N11 | N11: 48.pl | 79 | 6.03 | 0.57 | 14.03 | 0.26 | −1.26 | 0.64 | −1.29 | 0.07 | 82 |
| | N11: 49.pl | 84 | 6.01 | 0.57 | 14.08 | 0.26 | −1.31 | 0.64 | | | |
| N17 | N17: 50.pl | 77 | 5.58 | 0.57 | 13.83 | 0.26 | −1.62 | 0.64 | −1.62 | | |
| N21 | N21: 51.pl | 84 | 2.13 | 0.57 | 8.73 | 0.26 | −2.41 | 0.64 | −2.43 | 0.04 | 85 |
| | N21: 52.pl | 86 | 1.26 | 0.57 | 7.13 | 0.26 | −2.44 | 0.64 | | | |
| | | | | | | | sample mean: | | −2.01 | 1.21 | |

[a] analytical uncertainty

[b] variability

**Table 2.**

Mean oxygen three-isotope ratios and Mg#'s of chondrules in NWA 8613.

| Ch# | Type | | Olivine[a] | | Pyroxenes[a] | | | Mg#[c] | $\delta^{17}O$ | | $\delta^{18}O$ | | $\Delta^{17}O$ | |
|---|---|---|---|---|---|---|---|---|---|---|---|---|---|---|
| | | | Relict[b] | Host | LowCa | IntPx | HPx | Mean | Mean | Unc.[d] | Mean | Unc.[d] | Mean | Unc.[d] |
| N1 | I | POP | 3 | 4 | 4 | 2 | 3 | 98.2 | −4.30 | 0.25 | −1.04 | 0.34 | −3.76 | 0.17 |
| N2 | I | BO | - | 4 | 3 | - | 1 | 99.0 | −8.27 | 0.23 | −5.47 | 0.33 | −5.43 | 0.17 |
| N3 | I | POP | - | 4 | 3 | 2 | - | 98.9 | −6.61 | 0.22 | −3.35 | 0.33 | −4.87 | 0.14 |
| N4 | I | POP | 6 | 1 | 3 | 1 | - | 98.9 | −7.30 | 0.20 | −4.33 | 0.38 | −5.05 | 0.10 |
| N5 | I | PO | - | 4 | 2 | - | - | 99.0 | −8.19 | 0.27 | −5.47 | 0.36 | −5.35 | 0.20 |
| N6 | I | POP | - | 6 | 2 | - | - | 98.7 | −8.34 | 0.27 | −5.95 | 0.49 | −5.25 | 0.14 |
| N7 | I | POP | 3 | 1 | 4 | - | - | 98.8 | −8.02 | 0.25 | −5.41 | 0.33 | −5.21 | 0.22 |
| N8 | I | POP | 1 | 2 | 4 | - | - | 98.8 | −6.49 | 0.31 | −3.74 | 0.44 | −4.54 | 0.27 |
| N9 | I | PP | 2 | 1 | 5 | - | - | 99.0 | −7.93 | 0.23 | −5.41 | 0.33 | −5.12 | 0.17 |
| N10 | I | PO | - | 4 | 5 | - | - | 98.7 | −7.62 | 0.28 | −4.69 | 0.39 | −5.18 | 0.18 |
| N11 | I | POP | - | 1 | 4 | 1 | - | 98.7 | −7.80 | 0.42 | −4.78 | 0.55 | −5.32 | 0.24 |
| N12 | I | POP | 1 | 2 | 3 | - | 1 | 98.7 | −6.09 | 0.21 | −2.79 | 0.39 | −4.64 | 0.16 |
| N13 | I | PO | 3 | 3 | - | 1 | - | 99.0 | −5.06 | 0.62 | −2.90 | 0.80 | −3.55 | 0.25 |
| N14 | I | POP | - | 4 | 3 | - | - | 99.1 | −7.89 | 0.26 | −4.71 | 0.35 | −5.44 | 0.16 |
| N15 | I | BO | - | 3 | - | 5 | 2 | 91.0 | 1.68 | 0.23 | 3.42 | 0.32 | −0.09 | 0.16 |
| N16 | II | PO | 4 | 4 | - | - | - | 61.6 | −1.14 | 0.24 | 2.20 | 0.50 | −2.28 | 0.15 |
| N17 | I | POP | 2 | 3 | 4 | - | - | 98.8 | −6.19 | 0.35 | −3.20 | 0.46 | −4.52 | 0.18 |
| N18 | I | POP | - | 4 | 4 | - | - | 98.9 | −6.45 | 0.23 | −3.54 | 0.36 | −4.60 | 0.15 |
| N19 | I | POP | - | 4 | 4 | - | - | 99.1 | −9.06 | 0.28 | −6.13 | 0.35 | −5.87 | 0.20 |
| N20 | I | PO | - | 4 | 4 | - | - | 99.0 | −10.53 | 0.25 | −7.50 | 0.35 | −6.63 | 0.14 |
| N21 | I | POP | - | 4 | 3 | 1 | - | 98.9 | −7.94 | 0.23 | −4.63 | 0.33 | −5.53 | 0.14 |
| N22 | I | POP | - | 4 | 2 | 2 | - | 99.0 | −8.11 | 0.23 | −4.50 | 0.39 | −5.78 | 0.14 |
| N23 | I | POP | - | 4 | 2 | 2 | - | 98.7 | −6.44 | 0.21 | −3.25 | 0.41 | −4.75 | 0.17 |
| N24 | I | POP | - | 5 | 3 | - | - | 99.1 | −9.87 | 0.25 | −6.67 | 0.31 | −6.40 | 0.18 |
| N25 | I | POP | - | 4 | 5 | - | - | 99.2 | −9.00 | 0.21 | −5.57 | 0.32 | −6.10 | 0.15 |
| N26 | I | PP | - | 2 | 6 | - | - | 98.8 | −8.78 | 0.23 | −5.82 | 0.36 | −5.76 | 0.19 |
| N27 | I | POP | 2 | 2 | 3 | - | - | 99.0 | −10.53 | 0.26 | −7.45 | 0.33 | −6.66 | 0.19 |
| N28 | I | POP | - | 5 | 1 | - | - | 98.9 | −9.45 | 0.21 | −6.41 | 0.32 | −6.11 | 0.14 |
| N29 | I | POP | - | 4 | 3 | - | - | 98.8 | −7.40 | 0.30 | −4.38 | 0.41 | −5.12 | 0.20 |
| N30 | I | POP | - | 4 | - | 2 | - | 98.5 | −5.93 | 0.25 | −2.60 | 0.34 | −4.58 | 0.17 |
| N31 | I | POP | - | 4 | 4 | - | - | 98.9 | −7.77 | 0.39 | −4.64 | 0.51 | −5.35 | 0.20 |

[a] Number of analyses

[b] relict olivine not included in chondrule means

[c] Mg#'s of pyroxenes, except for chondrule N16

[d] for calculation of uncertainty see Section 2.5